Journal of Natural Fibers

ISSN: 1544-0478 (Print) 1544-046X (Online) Journal homepage: www.tandfonline.com/journals/wjnf20

Highly Conductive Nanocellulose–Polyaniline Nanocomposites for Efficient Heavy Metal Adsorption and Regeneration

Nur Athirah Abdullah, Mohd Saiful Asmal Rani, Masita Mohammad, Muhamad Fadhli Ramlee & Rushdan Ahmad Ilyas

To cite this article: Nur Athirah Abdullah, Mohd Saiful Asmal Rani, Masita Mohammad, Muhamad Fadhli Ramlee & Rushdan Ahmad Ilyas (2026) Highly Conductive Nanocellulose–Polyaniline Nanocomposites for Efficient Heavy Metal Adsorption and Regeneration, Journal of Natural Fibers, 23:1, 2628738, DOI: 10.1080/15440478.2026.2628738

To link to this article: https://doi.org/10.1080/15440478.2026.2628738

Published online: 20 Feb 2026.

JOURNAL OF NATURAL FIBERS
2026, VOL. 23, NO. 1, 2628738
https://doi.org/10.1080/15440478.2026.2628738

Taylor & Francis
Taylor & Francis Group

Highly Conductive Nanocellulose–Polyaniline Nanocomposites for Efficient Heavy Metal Adsorption and Regeneration

Nur Athirah Abdullah[a], Mohd Saiful Asmal Rani[a,b], Masita Mohammad[c], Muhamad Fadhli Ramlee[c], and Rushdan Ahmad Ilyas[d,e]

[a]Department of Physics, Faculty of Science, Universiti Putra Malaysia, Serdang, Malaysia; [b]Institute of Tropical Forestry and Forest Products (INTROP), Universiti Putra Malaysia, Serdang, Malaysia; [c]Solar Energy Research Institute (SERI), Universiti Kebangsaan Malaysia, Bangi, Malaysia; [d]Faculty of Chemical and Energy Engineering, Universiti Teknologi Malaysia UTM, Johor Bahru, Malaysia; [e]Centre for Advanced Composite Materials, Universiti Teknologi Malaysia UTM, Johor Bahru, Malaysia

ABSTRACT

Polyaniline (PANI) is extensively researched for its conductivity and enhanced properties for multifunctional commercial applications, addressing heavy metal pollution. This work details the synthesis of nanocellulose/copper ions (NCs-Cu^{2+}) doped PANI nanocomposites via in-situ polymerization which assesses the nanocomposites' efficiency in heavy metal adsorption and their regenerability. NC extraction employs acid hydrolysis, while batch adsorption experiments consider parameters like pH, adsorbent dosage, Cu^{2+} concentration, and contact time. Nanocomposites are prepared using different ratios to compare conductivity (1:9, 2:8, 3:7) and characterized using XRD, FESEM, TEM, FTIR, and TGA. XRD reveals increased ordering with NC-Cu^{2+} concentration, indicating a highly ordered PANI structure in the presence of NC-Cu^{2+}. FESEM shows morphological changes and homogenous nano dispersion. TEM depicts rod-like NC-Cu^{2+} PANI structures. FTIR demonstrates slight peak shifts during in-situ polymerization and TGA confirms its high thermal stability. Adsorption mechanisms are studied with Langmuir and Freundlich isotherms, showing good agreement between experimental and theoretical data. The conductivity of NC-Cu^{2+}PANI ranges from 5.73 to 18.27×10 S/cm^{-1}, significantly higher than pure PANI (3.53×10 S/cm^{-1}), with a decrease in conductivity as the NC-Cu^{2+}-to-PANI ratio increases. This research provides insights into the synthesis, properties, and applications of PANI-based nanocomposites for heavy metal removal.

摘要

聚苯胺 (PANI)因其导电性和增强的性能而被广泛研究，可用于多功能商业应用，解决重金属污染问题. 这项工作详细介绍了通过原位聚合合成纳米纤维素/铜离子 (NCs-Cu^{2+})掺杂的PANI纳米复合材料，评估了纳米复合材料在重金属吸附方面的效率及其可再生性. NC提取采用酸水解，而批量吸附实验考虑了pH值、吸附剂用量、 Cu^{2+}浓度和接触时间等参数. 使用不同的比例制备纳米复合材料以比较电导率 (1:9、2:8、3:7)，并使用XRD、FESEM、TEM、FTIR和TGA进行表征. XRD显示，随着NC-Cu^{2+}浓度的增加，有序性增加，表明在NC-Cu^{2+}存在下，PANI结构高度有序. FESEM显示形态变化和均匀的纳米分散. TEM描绘了棒状NC-Cu^{2+}PANI结构. FTIR在原位聚合过程中显示出轻微的峰移，TGA证实了其高热稳定性. 用Langmuir和Freundlich等温线研究了吸附机理，实验数据和理论数据之间具有良好的一致性. NC-Cu^{2+}PANI的电导率范围为5.73至18.27×10 S/cm^{-1}，明显高于纯PANI (3.53×10 S/cm^{2})，电导率随着NC-Cu2±与PANI比率的增加而降低. 本研究为PANI基纳米复合材料的合成、性能和重金属去除应用提供了见解.

KEYWORDS
Polyaniline; nanocellulose; in situ polymerization; conductivity

关键词
聚苯胺; 纳米纤维素; 原位聚合; 导电性

Introduction

Agricultural biomass has long been recognized as a valuable source of natural raw materials that may be converted into a variety of value-added products (Gupta et al. 2022). Agricultural biomass includes all organic materials such as leaves, straws, husks, hulls and shells, which are abundant, affordable, sustainable and viable. These wastes have a lot of advantage as a raw material for making biochemicals and biofuels without competing with human food supplies (Clauser et al. 2021). These materials have been presented as

CONTACT Mohd Saiful Asmal Rani saifulasmal@upm.edu.my Department of Physics, Faculty of Science, Universiti Putra Malaysia, Serdang, 43400, Malaysia

a potential answer to pollution and energy shortages. Numerous studies from across the world have been documented the value of various forms of agro-waste for diverse purposes. Figure 1 illustrates several types of agricultural wastes that can be utilized for value-added applications.

Nanocellulose fiber (NCF) are extracted from agricultural wastes through multi step treatment processes. The benefits of cellulose nanoparticles known as nanocelluloses (NCs) with physiochemical features are much better compared to cellulose (Trache et al. 2020). NC is renewable, abundant, chemically inert, posses high mechanical strength, excellent stiffness and low density (Köse, Mavlan, and Youngblood 2020; Naz, Ali, and Zia 2019; Phanthong et al. 2018). Moreover, NCs particles including nanocellulose crystal (NCC) and NCF can be obtained from different agricultural biomass through different treatment methods (Pires, Souza, and Fernando 2019). The research on fabrication of NCs particles comprising various features is considered an exciting and open topic Table 1.

Acid hydrolysis is used to extract NCs from cellulose fibers (Trache et al. 2017). A typical extraction technique begins with alkali pretreatment and bleaching, followed by defibrillation, which comprises acid hydrolysis to eliminate the amorphous parts of cellulose fibers, resulting in short rod-shaped NCs with increased crystallinity (Moberg et al. 2017). According to research, NCs have a rod-like shape and a chemical made up of 100% cellulose, predominantly in crystalline sections, with a high specific surface area of around 150 $m^2.g^1$ (Kaboorani and Riedl 2015). NCs with these features have potential for various applications (Köse, Mavlan, and Youngblood 2020; Vilarinho et al. 2017). Depending on the types of biomasses and the extraction procedure, the critical characteristics such as crystallinity, dimension, surface area, and surface shape may change (C. Liu et al. 2016). NCs with a higher crystallinity generally have better mechanical and thermal characteristics (Yang et al. 2017). More recently, NCs – based materials have found increasing industrial interest in biomedical applications, papermaking and in decontamination as adsorbent.

NCs also have found many applications in decontamination and water treatment due to their surface characteristics (Köse, Mavlan, and Youngblood 2020). They provide an environmentally acceptable technique for treating wastewater effluent that comprises heavy metals, dyes, and salts (Mahfoudhi & Boufi., Mahfoudhi and Boufi 2017). Due to the large surface area and porosity of NCs, large cadmium adsorption (Cr^{6+}) and lead (Pb^{2+}) were recorded (Wang et al. 2013). Fan et al. (2019)

Figure 1. Types of agricultural Wastes.

Table 1. Chemical characteristics of CHFs.

Ref.	Cellulose (%)	Lignin (%)	Hemicellulose (%)	Pectin/Wax (%)	Ash (%)	Moisture content (%)
Zainudin et al. (2014)	32–43	40–45	0.15–0.25	–	–	–
Narendar and (Dasan 2014)	27.41	42.0	14.63	10.16	–	–
Verma et al. (2013)	37	42	–	–	–	–
Malkapuram, Kumar, and (Negi 2009)	36–43	41–45	10–20	3–4	–	–
Barbosa et al. (2010)	43.4	48.3	4.0	–	3.5	10.2
Salleh et al.	39.3	49.2	2	–	–	9.8

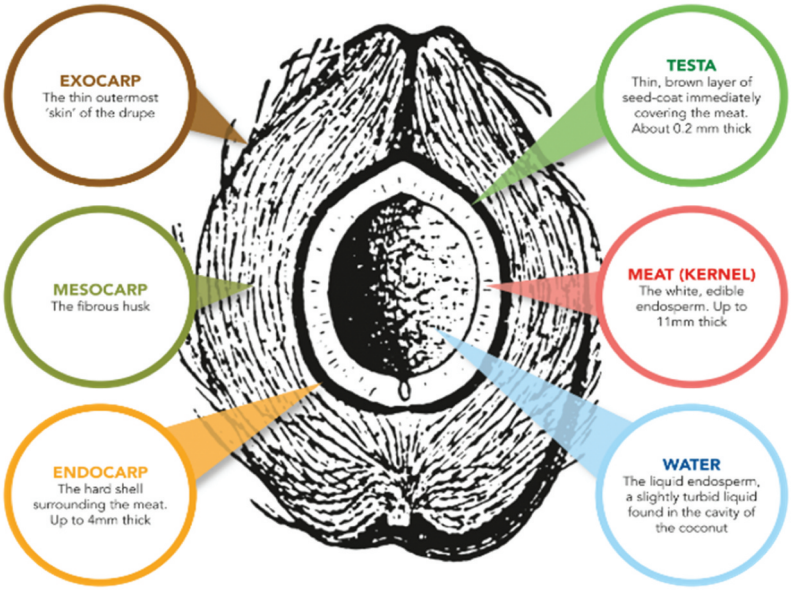

Figure 2. Coconut layers and Constituents.

prepared NCs with high carboxylation content for removal of Cu^{2+} from wastewater. Oyewo et al. (2019) reported highly efficient adsorption of cadmium (Cr^{6+}) and nickel (Ni^{2+}) using NCs from sawdust. NCs surface chemistry can be enhanced by grafting ionic and cationic functional groups such as sulfate (SO_3), carboxyl (COO^-), and amine ($-NH_2$) to meet wastewater treatment needs (Abouzeid et al. 2018).

Coconut husk fiber (CHF) is one of the most prevalent agricultural wastes and has been utilized for a variety of applications among the available lignocellulosic biomass (Jain, Rastogi, and Chanana 2022; Vakili et al. 2014). Defibrilation process of CHFs is simple and inexpensive. These flexible and strong fibers have high mechanical strength and thermal conductivity with low density (Hu et al. 2018). The different concentrations of lignin contain in CHFs influence the variable mechanical and physical properties and make the fibers more durable. These components consist primarily of carboxyl, hydroxyl, and ether groups, which make CHFs a useful adsorbent (Höfer 2015). Accordingly, CHFs are currently used by scientists and industries to discover more convenient methods for utilization in different applications. Coconuts are produced as a permanent crop in many regions of the world, particularly in tropical and sub-tropical climates. As a result, it is available all year as a consistent year-round supply, allowing it to play a vital role in economic growth (Haque, Akbar, and Kinnear 2020). According to report (Siakeng et al. 2019), 2 million tons of fibers obtained from 40 million tons of CHFs, thus it serves as a good candidate to replace conventional synthetic and natural fibers in composite materials. Figure 2 shows the coconut layer and constituents while Table 1 tabulates the chemical characteristics of CHFs.

Despite all the research, studies on CHFs are still limited. This research is about potential applications of CHFs for extraction of nanocelluloses (NCs) for further applications in adsorption of heavy metals for environmental decontamination and synthesis of renewable materials-based energy devices. Adsorption has been known as an attractive, simple, and inexpensive route for removal of heavy metals from wastewater containing low concentration of pollutants (Vardhan, Kumar, and Panda 2019). A group of researchers has critically evaluated the suitability of adsorption method in heavy metal removal and described adsorption as an excellent operative method due to its easy operating procedure and low cost compared to other approaches (Afroze and Sen 2018). The polymer composites containing polyaniline (PANI) are mostly investigated for blending with commercial polymers to obtain improved processability and good mechanical properties together with good conductivity for practical applications (C. Liu et al. 2016). However, the electrical conductivity of the composite was not improved effectively; especially the composites became more brittle due to addition of PANI (C. Liu et al. 2016). Cellulose fibers have been used to reinforce brittle conducting polymers, such as polypyrrole (PPy), PANI and polythiophene (PTP) for energy storage

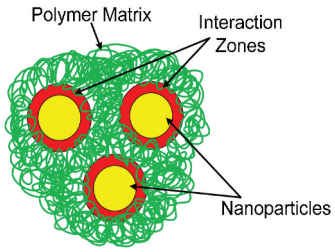

Figure 3. Diagram to illustrate the constituents of polymer nanocomposites.

applications (D. Y. Liu, Sui, and Bhattacharyya 2015). Figure 3 shows diagram illustrates the constituents of polymer nanocomposite.

Conductive materials can be mixed with nanocellulose (NCs) to form a new composite that combines the advantages of both components. Conductive materials include conductive polymers, conductive carbon compounds (carbon nanotubes, graphene, carbon black, and so on), and metallic particles with variable degrees of conductivity (Zhang et al. 2019). Nanocellulose is primarily utilized as a reinforcing component in composites to increase their physical strength (Mondal 2018). Nanocellulose-based conductive polymers combine the electrical capabilities of conductive polymers with the structural benefits of nanocellulose to produce composites for a wide range of applications (Shi et al. 2015). Mechanical and chemical stability and flexibility should be prioritized in the preparation of NCs-based conductive composites with the highest level of electrical conductivity. These conductive polymer composites are mostly used for energy storage (Dutta et al. 2017; Salado, Lanceros-Mendez, and Lizundia 2021; Shi et al. 2015) and electronic devices (Fei et al. 2019). The typical manufacturing techniques for nanocellulose (NC)-based conductive composites are depicted in Figure 4.

The process of developing effective adsorbents for pollutant removal has evolved significantly, spanning from early studies focused on basic materials to the advanced, tailored adsorbent systems of today. Historically, research began with traditional adsorbents such as activated carbon and zeolites, which were widely used in industrial applications for their ability to remove heavy metals and organic compounds from water and air. However, the need for more sustainable, efficient, and multifunctional adsorbents has driven the development of newer materials. Recent studies have explored a variety of adsorbent types, including biopolymer-based materials, nanomaterials, and composite adsorbents, which offer superior surface areas, enhanced mechanical properties, and selective adsorption capabilities (El Messaoudi, Miyah, Singh, et al. 2024). These innovations have significantly advanced the field, allowing for more efficient removal of pollutants, such as toxic heavy metals, dyes, and pharmaceuticals from wastewater, as well as applications in air purification and soil remediation (Ahamad and Nasar 2025; El Messaoudi, Miyah, Wan, et al. 2024). The present scope of research is heavily focused on enhancing the functionalization of adsorbent materials through surface modifications, improving their recyclability, and ensuring their environmental sustainability. Looking ahead, the future of adsorbent

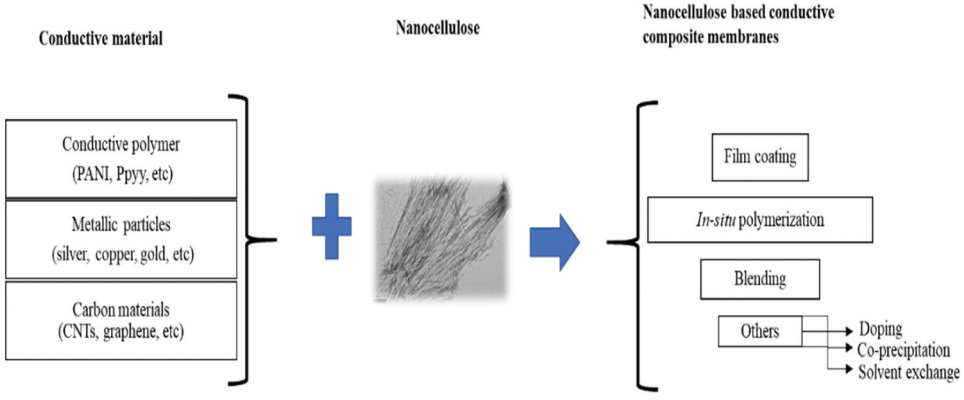

Figure 4. Nanocellulose (NCs)-based conductive composite fabrication routes.

technology lies in the development of smart adsorbents with tailored properties for specific pollutants, as well as scaling up production for industrial applications (Khan, Ahamad, and Nasar 2025). As industries continue to face growing challenges related to environmental pollution, these advanced adsorbent materials, derived from sustainable sources and engineered for optimal performance, offer promising solutions for addressing water, air, and soil pollution (Aasli et al. 2025; Ahamad and Nasar 2025). Therefore, this body of work not only reflects the progress made in adsorbent research but also highlights the significant potential for future developments in the field, positioning adsorbents as central components in environmental sustainability and industrial pollution control.

In this work, CHFs are explored as a sustainable and low-cost precursor for the extraction of NCs via a sequence of chemical treatments, namely alkaline treatment, bleaching, and acid hydrolysis. The novelty of this study lies in the systematic linkage between NCs extraction from CHFs, detailed structural characterization (chemical composition, XRD, FESEM, TEM, FTIR, TGA, AAS), and their subsequent use in Cu(II) adsorption and nanocomposite conductivity testing. By investigating the effects of key operating parameters – initial Cu(II) concentration, contact time, pH, and NC dosage – and analyzing the adsorption kinetics to identify optimum conditions, this work provides an integrated framework that connects green nanocellulose production from agricultural waste with its functional application in heavy metal removal and conductive nanocomposite development.

Methodology

Materials

CHFs were collected from agricultural holdings in Sabak Bernam, Malaysia as well as from night market and weekly market in Section 16, Bandar Baru Bangi. A total of 2 bags or 3 kg of samples were collected in this study. These samples were completely dried before grinding into smaller pieces or sizes (0.3 mm). Reagent grade chemicals used for pre-treatment, namely toluene, ethanol, sodium chlorite and pottasium hydroxide, have been obtained from R&M Chemicals, United Kingdom. Sulfuric acid used in this experiment for the extraction of nanocellulose was purchased from R&M Chemicals, United Kingdom. All analytical grade solvents have been purchased from R&M Chemicals, United Kingdom. Analytical grade copper (II) nitrate was obtained from R&M Chemicals, United Kingdom and was used for copper ion sources. ACS Reagent grade concentrated nitric acid and sodium hydroxide were derived from Aldrich and used to adjust the pH values of the samples. The pH buffer solutions have been obtained from Aldrich Chemical Company and Chemlab Supply Co. All experimental work used distilled water from running distilled water at lab.

Preparation of nanocellulose from coconut husk fibers

Alkali pre-treatment of coconut husk fibers

CHFs were pre-treated before cellulose extraction took place. For alkali-treated CHFs, these fibers were washed three times with tap water to remove debris, dust, and contaminants and dried at room temperature for 48 h. It was then cut into small pieces and dried in a drying oven at 60°C for 48 h. Dry CHFs were then immersed in 5 wt.% NaOH solution at a lab temperature of 25°C for 30 min, followed by washed 10 times with fresh water to allow the absorbed alkali to leach from the fibers. These washed fibers were then naturally dried for 24 h and then dried for 8 h at 50°C in the oven. Finally, the dried fibers were sealed in a plastic bag prior to the composite manufacture to avoid contamination of atmospheric moisture. Dry samples were ground using a grinder machine and the powder was obtained in size 0.3 mm. These samples were then extracted with 2:1 v/v toluene ethanol for 6–8 h to remove wax and oils using the Soxhlet apparatus and then dried in the oven at 60°C. The samples were stored in a polyethylene plastic bag and placed at room temperature for further processing. The alkali treatment provides several advantages. Low temperature/pressure performance led in efficient and cost-effective NCC extraction from waste materials. However, careful process control is required to avoid undesired cellulose breakdown. Researchers are paying close attention to CHFs, which are one of several renewable resources.

Extraction of cellulose (MCC)

The method used in this study was adopted with a slight modification (Sun et al. 2004). Fifteen grams of samples were placed in a 1.0 L beaker and 500 mL of sodium chlorite was added, in a water bath for 1 h at 70°C. These samples were delignified with 2% w/v sodium chlorite in the pH range of 3.5–4.0, adjusted using 10% acetic acid. This process was repeated three times and washed thoroughly with distilled water and filtration. It was then treated with 6% wt. aqueous dilution of potassium hydroxide for 24 h and subsequent washed with water until pH 7, the procedure was repeated for the remaining samples. The resulting cellulose was thoroughly washed with distilled water. The cellulose material obtained was filtered and dried in oven at a temperature of 60°C for 1 h.

Extraction of nanocellulose (NCs)

The isolation of NCs was performed using the acid hydrolysis method following the work reported by (Morán et al. 2008) with minor modifications. Briefly, the obtained CHFs (10 g) was hydrolyzed in 64% (w/w) of sulfuric acid at a liquor ratio of 1:20 g/mL and 50°C for 45 min under vigorous and constant stirring. Subsequently, the sample obtained was diluted by adding tenfold of cold distilled water and then centrifuged at 10,000 rpm for 30 min. After discarding the supernatant, the sample was collected and washed continuously with cold distilled water and then again centrifuged. The process of centrifuge was repeated until the supernatant turned clear (6 cycles of centrifuging). The suspension collected was dialyzed against distilled water for 5 days until the pH was constant (pH 5). The resulting suspension was finally ultrasonic for 30 min and stored at 4°C for further use. NCs obtained were freeze dried at-50°C for 24 h and were sealed for further use.

Preparation of NC/Copper (ii) nitrate (NCs-CU^{2+})

Copper (II) nitrate solutions have been prepared from the stock solution to study their removal using NCs using adsorption. The general method used for this study is described as follows;

0.5, 1.0, 2.0, 3.0 and 4.0 g of NCs were added to five different flasks each containing 100 ml of copper (II) nitrate without any pH adjustment. The mixture of the Cu^{2+} solution and NCs was stirred continuously in a shaker at 70 rpm for 3 h. Separate samples for copper were taken at intervals of 10, 40, 80, 120 and 180 min. After stirred, the suspension was centrifuged in the stop tube for 2 min at 2000 rpm and the metal solution was then analyzed using the atomic adsorption spectrometer (AAS). The effect of several parameters on adsorption, such as pH, concentrations, contact time and quantity of NCs was studied. The suspension pH of one set of experiments was adjusted with NaOH and HNO_3. The adsorption of copper on the walls of glass flasks and centrifugal tubes, which was found to be negligible, was determined by the use of blank experiments.

Effect of pH

The effect of pH on copper sorption on NCs was investigated at room temperature by varying the pH of NCs-Cu^{2+} suspension from 2.0 to 10. For this purpose, 0.30 g NCs sample was added to each 100 mL volume of copper solution having an initial concentration of 100 mg/L at a constant adsorption time of 180 min.

Effect of adsorbent dosage

The dependence of copper sorption on the concentration of NCs was studied at room temperature and fixed pH values (pH 6) by varying the sorbent amount from 0.5 g to 4.0 g while keeping the volume (100 ml) of the metal solution constant.

Effect on initial concentration of copper (II) nitrate and contact time

A sample of 0.5 g of NCs was added to each 100 mL of copper solution. The initial concentrations for copper (II) nitrate tested were 20, 40, 60, 80 and 100 mg/L.

Adsorption isotherm

The adsorption isotherms for Cu^{+2} on NCs were investigated at pH 6.0 and 25°C. Sample of 8 g/L of NCs were added in centrifuge tube and mixed with 25 mL Cu^{+2} with the initial concentration's levels of 0, 5, 10, 25, 50, 100, 200 and 400 mg/L. The 1 mol/L KNO_3 solutions were applied to adjust the ionic strength to 0.1 mol/L, and the centrifuge tubes were shaken at 120 rpm for 12 h. The adsorption isotherms were simulated using the Langmuir and Freundlich models.

Langmuir adsorption isotherm model was usually adopted for homogenous adsorption for monolayer adsorption process. Linear form of Langmuir model was expressed by:

$$\frac{C_e}{q_e} = \frac{1}{Q_0 b} + \frac{C_e}{Q_0} \tag{1}$$

where C_e is equilibrium constant of Cu^{2+} q_e (mg/l), is the amount of Cu^{2+} adsorbed at equilibrium (mg/g), Q_0 is the Langmuir constant related to adsorption capacity (l/mg).

The Langmuir model describes quantitatively the formation of a monolayer adsorbate on the outer surface of the adsorbent; thus, no further adsorption takes place (Lani et al. 2014). It represents the adsorbate uptake that occurs on a homogeneous monolayer with no interaction between the adsorbed ions.

The characteristic of Langmuir model best described by separation factor or equilibrium parameters R_L; where C_0 is the initial Cu^{2+} concentration, mg/l. The value of separation factor indicated the nature of adsorption process as given in Table 2.

The Freundlich adsorption model is one model in describing sorption related to heterogeneous system. It is known to be satisfactory empirical isotherm that can be used for non-ideal sorption for the said system. The empirical equation can be expressed in its logarithmic form:

$$q_e = K_F + \frac{1}{n} \ln c_e \tag{2}$$

where q_e is the amount adsorbed (mg/g), C_e is the equilibrium concentration of the adsorbate (Cu^{2+}) (mg/l), K_F and n are Freundlich constant. Value of n will give indication of how favorable the adsorption process is.

The Freundlich adsorption model is one model in describing sorption related to heterogeneous systems. It is known to be satisfactory empirical isotherm that can be used for non-ideal sorption for heterogeneous system.

Adsorption mechanism

Kinetic experiment was conducted with 8 g/L NCs samples and 25 mL metal solution with the predetermined concentrations of 100 mg/L. The mixtures were shaken continuously at 25°C and the rate of 125 rpm with the solution pH 6.0. The samples were taken at intervals and immediately centrifuged and filtered. The equilibration times were set from 5 min to 180 min. The adsorption behaviors and adsorption kinetics of NCs were investigated.

The adsorption of solute in an aqueous solution is a process with often complex kinetics. The adsorption rate is strongly influence by several parameters. To study the adsorption of Cu^{2+} on NCs, kinetic adsorption

Table 2. Separation factor, R_L.

R_L Value	Nature of adsoprtion process
RL > 1	Unfavourable
RL = 1	Linear
0 < RL < 1	Favorable
R_L = 0	Irreversible

data obtained were fitted into two different kinetic models. First, experimental data were fitted with pseudo-first-order kinetic model:

$$\frac{dq_t}{dt} = k_1(q_e - q) \tag{3}$$

The first order-rate constant k_1 can be obtained from the slope of the plot log (q_e-q_t) vs. time. Kinetic data were further fitted with pseudo-second-order kinetic model:

$$\frac{dq_t}{d_t} = k_1(q_e - q)^2 \tag{4}$$

where k_1 is the equilibrium rate constant of pseudo-second-order adsorption (g/mg min). Equation for the boundary conditions $t = 0$ to $t = t$ and $qt = 0$ to $qt = qt$ and rearrangement give the following linear form:

$$\frac{t}{q_t} = \frac{1}{k_2 {q_e}^2} + \frac{1}{q_e}t \tag{5}$$

The slope and intercept of the plot t/qt versus t were used to calculate the second order rate constant, k_2.

PANI/Nanocellulose/Metal ions (NC-Cu^{2+}PANI)

Various amounts of aniline have been dissolved in 1 M hydrochloric acid (HCl) in an ice bath. In a separate conical flask, NCs-Cu^{2+} was dispersed in deionized water (DIW) and stirred moderately until the mixture became homogeneous. 0.2 g HCl/aniline solution and 0.44 g ammonium persulfate (APS) were dissolved in distilled water. HCl/aniline solution was added to NCs-Cu^{2+} aqueous suspension (0.5 wt%) followed by a dropwise addition of APS. The weight ratio for HCl/aniline solution and nanocellulose is 1:9, 2:8 and 3:7. The mixture was kept stirred at room temperature for 24 h and then diluted and washed with deionized water. The green emeraldine polyaniline nanocomposite (NCs-Cu^{2+}PANI) precipitate was filtered out and washed with distilled water at least 3 times under centrifugation until the supernatant was clear. The mixture was applied directly to the petri dishes. The precipitate was dried in the oven at 60°C for 6 h. PANI was prepared under the same condition for the purpose of comparison.

Results and discussion

The chemical composition of CHFs at various stages of processing is shown in Table 3. According to Table 3, the original CHFs contained 53.98% cellulose, 30.14% lignin, 7.52% hemicellulose, 0.98% ash, and 2.35% extract. When treated with a $NaClO_2$ solution, the cellulose content in CHFs increased by 28.35% and lignin decreased by 29.87%. After the third bleaching, a significant amount of lignin was obtained with a cycle time of 1 h. Using $NaClO_2$ initially is an excellent choice for lignin removal since natural fibers can be viewed as a composition of cellulosic fibers trapped in lignin as a binder in a hemicellulose matrix (Phanthong et al. 2018). As a result, the hemicellulose is easier to be removed after removing the lignin. Alkaline treatment led to a significant decrease in the content of hemicellulose in the fibers from 7.52% to 3.78%. The bleaching treatment dissolved the lignin, while the remaining hemicellulose and lignin fibers dissolved in the dilute alkali treatment, which makes the lignin more susceptible to hydrolysis. In addition, as shown in Table 3, from the CHFs, most of the lignin and hemicellulose were removed by chemical treatment. The amount of lignin decreased from 30.14% to 0.27%, and the amount of hemicellulose decreased from 7.52% % to 3.78%, and the amount of cellulose increased from 53.98% to 82.33%.

Table 3. Chemical composition of coconut husk fiber.

Coconut husk fiber content	Chemical composition (%) (Before treatment)	Chemical composition (%) (After treatment)
Cellulose	53.98	82.33
Hemicellulose	7.52	3.78
Lignin	30.14	0.27
Extractives	2.35	N/A
Ash	0.98	N/A

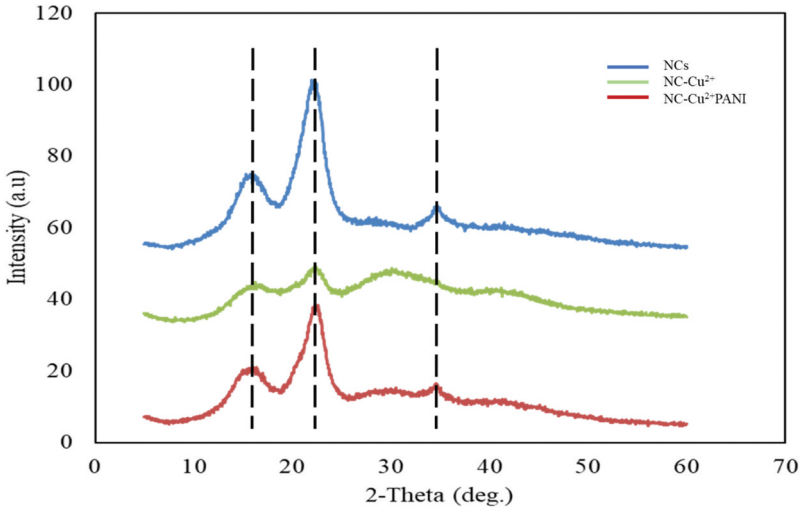

Figure 5. X-Ray diffractogram of NCs, NC-Cu^{2+} and NC-Cu^{2+}PANI.

X-Ray diffraction (XRD)

To study the crystallinity of the synthesized materials, XRD pattern was performed as shown in Figure 5. Figure 5 shows the X-ray diffraction (XRD) measurements of NCs, NC-Cu^{2+} and NC-Cu^{2+}PANI obtained under different conditions which is acid hydrolysis of NCs, batch adsorption of NC-Cu^{2+} and *in-situ* polymerization of NC-Cu^{2+} PANI respectively and Figure 6 shows the chemical structure of NCs, NC-Cu^{2+} and NC-Cu^{2+}PANI.

XRD pattern of NCs, NC-Cu^{2+} and NC-Cu^{2+}PANI are shown in Figure 5. Each sample showed three distinct peaks of cellulose at 2θ values of 16.4°, 22.73° and 35.07°. These three peaks with the major intensified peak at 2θ = 22.8° are characteristic to the NCs, attributed to crystallographic planes 110, 200 and 004, respectively (Rashid and Dutta 2020). Removal of non-cellulosic components during extraction process can cause shifting of XRD peaks (Monte et al. 2018). The Van der Waals forces and hydrogen bonds that act in the crystalline zones of the cellulose provide high resistance to acid attack, while the amorphous regions are disordered and prone to sulfuric acid hydrolysis (Collazo-Bigliardi, Ortega-Toro, and Boix 2018). Thus, the sulfuric acid treatment removes the cellulose fibers of the amorphous zones and reduces the fiber size to nanometric scale (Chieng et al. 2017). In this study, no such shifting was observed which indicates that lignin and hemicellulose did not cause any hindrance in the native crystalline form of cellulose in the husk samples.

The XRD pattern of NC-Cu^{2+} (Figure 5) shows the characteristic peaks of Cu^{2+} confirms the presence of Cu^{2+} in the composite. However, the XRD patterns of NC-Cu^{2+}PANI composites exhibit the characteristic

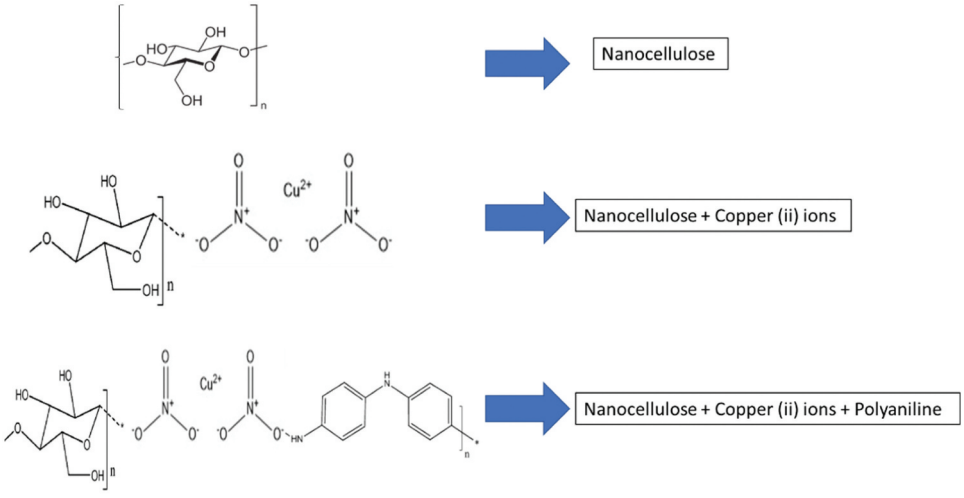

Figure 6. Molecular structure of NCs, NC-Cu^{2+} and NC-Cu^{2+}PANI.

peak of PANI along with the crystalline peaks of NC-Cu^{2+}, owing to the systematic alignment of polymer chain (Sangamesha, Pushpalatha, and Shekar 2014). This could be because of the amorphous PANI and the association of NCs and Cu^{2+}. The increase in ordering of polymer composite with the addition of NC-Cu^{2+} nanoparticles indicates that the structure of PANI is strongly influenced by the molar concentration of nanoparticles. This implies that the molecular chain of synthesized PANI composite is in a highly ordered state in the presence of NC-Cu^{2+}.

The increase in degree of regularity in arrangement or ordering of polymer chain is due to the strong interfacial interaction between the polymer and nanoparticles (Ramesan 2014). Hence, the orientation of conducting polymer nanocomposites is of much interest, because more highly ordered polymer matrix could display a conductive property such as metallic state.

Field emission scanning electron microscopy (FESEM)

Figure 7 shows FESEM micrographs of NCs, NC-Cu^{2+}, and NC-Cu^{2+}PANI and Figure 8 shows FESEM-EDX image of NC-Cu^{2+}PANI.

It can be observed from FE-SEM micrograph Figure 7(a, b, c) that surface of NCs showed irregularities and after adsorption Figure 7(d, e, f) there were clusters or agglomerations of copper on the nano-adsorbent (nanocellulose synthesized from coconut husk fiber) surface confirming the adsorption of copper. NC-Cu^{2+} showed a bulky, granular, and dense structure Figure 7(d, e, f) but a remarkable change from bulky and shapeless structure to granular like structure was observed upon addition of PANI to the structure Figure 7(g, h, i), proving the polymerization of aniline on the cellulose surface. The features of the NC-Cu^{2+} composite changed slightly to a granular like structure on further addition of PANI whereupon the fibers become less agglomerated. The proper mixing of NC-Cu^{2+} and PANI combines the nanostructure advantage of biopolymer and the electrical properties of PANI explaining the higher anodic current obtained for the composite. The significant change in the morphology of nanocomposite (NC-Cu^{2+}PANI) reveals the homogenous nano dispersion in the PANI matrix and this morphology clearly noticed that their average diameter of structure is about 70–100 nm. These changes in the structure may confirm the effect of nano in the polymer matrix.

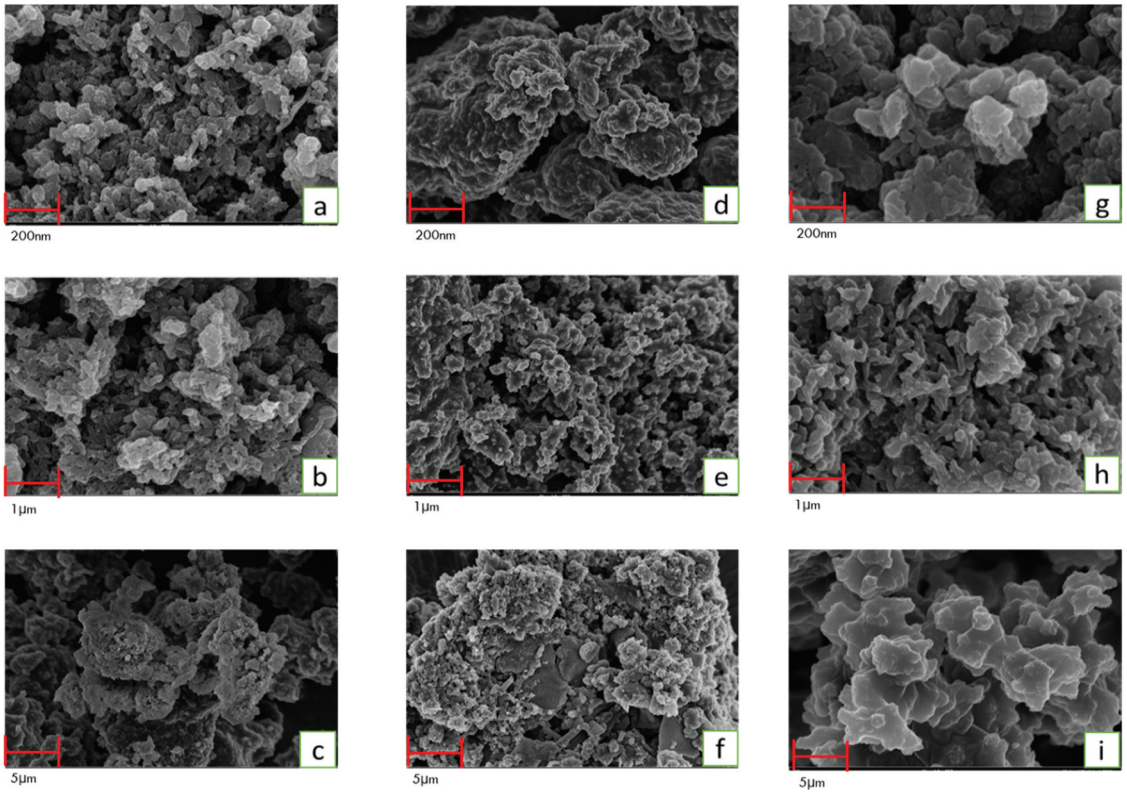

Figure 7. FESEM micrographs of NC (a,b,c), NC-Cu^{2+}(d,e,f), NC-Cu^{2+}PANI (g,h,i).

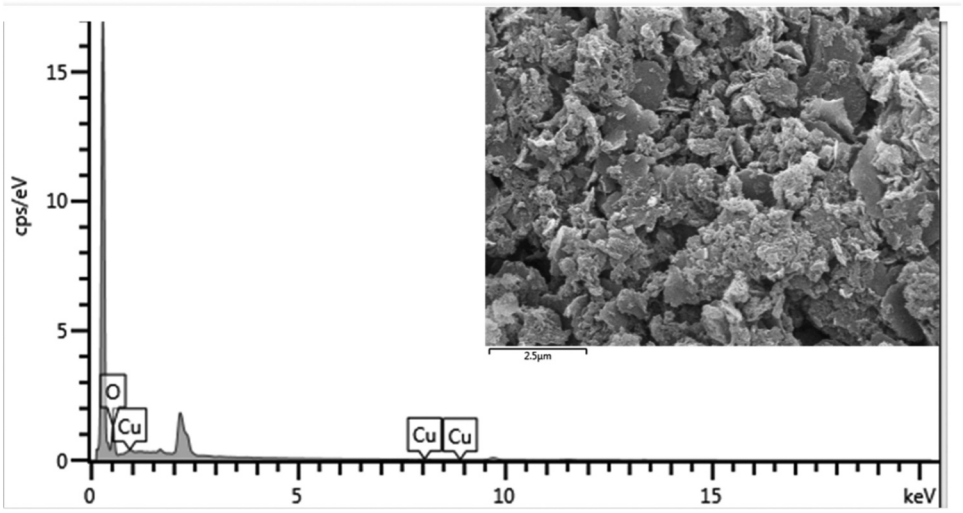

Figure 8. FESEM-EDX image of NC-Cu^{2+}PANI.

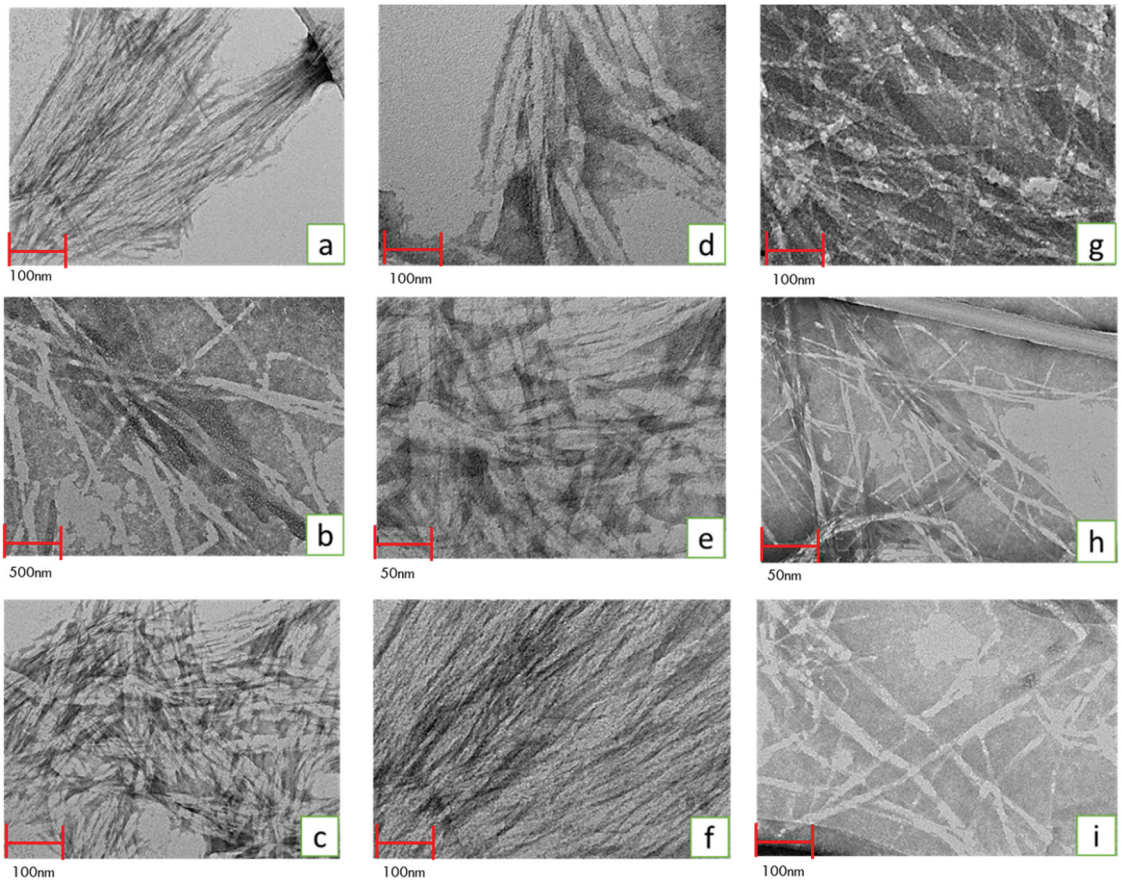

Figure 9. TEM images of NCs, NC-Cu^{2+} and NC-Cu^{2+}PANI.

Transmission electron microscopy (TEM)

Figure 9 depicts TEM micrographs of NCs, NC-Cu^{2+} and NC-Cu^{2+}PANI prepared under various conditions which is acid hydrolysis, batch adsorption and *in-situ* polymerization respectively.

From Figure 9(a, b, c) the NCs exhibited rod-like structure, at 10–20 nm in width and 100–350 nm in length, which is the typical measurements found in nanocellulose. When acid hydrolysis takes place,

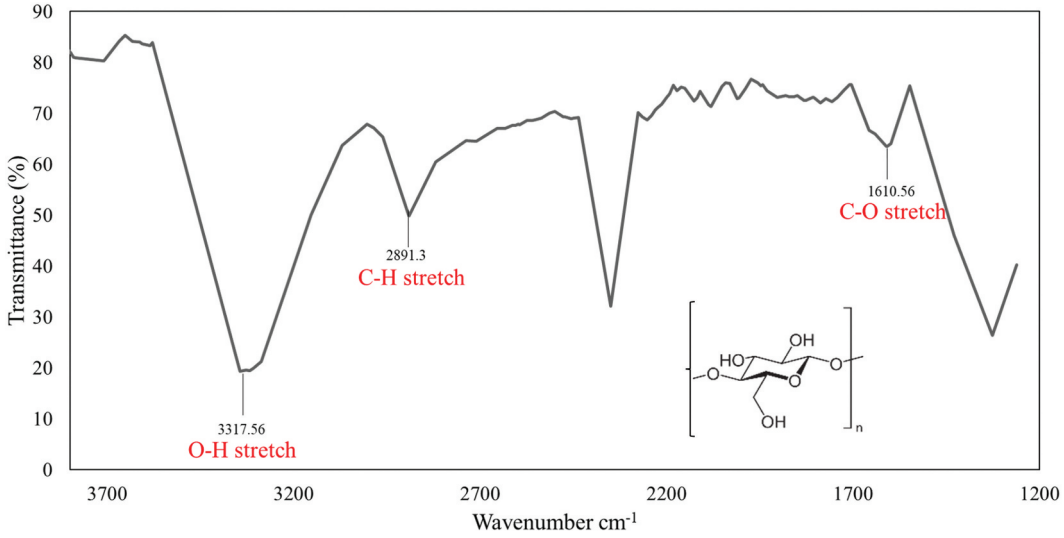

Figure 10. FTIR of NCs.

amorphous portions of the long chain cellulose are preferably hydrolyzed, while the crystalline regions having higher resistance to acid attack, hence producing rod-like particles, NCs in nanoscale region (Khoo, Ismail, and Chow 2016). Based on these findings, acid hydrolysis can effectively reduce a large amount of fiber sizes (from micron-size to nano-size), which agrees with previous findings by other authors (Septevani et al. 2020; Song et al. 2018). On top of that, the cellulose rods were agglomerated in some places while in some other regions they are separated. The analysis of the TEM micrograph revealed that the aqueous suspension of nanocellulose fiber consists of rodlike nanoparticles, whereby there were some nanoparticles agglomerated in the forms of bundles while some of them were well separated. The agglomeration is generally due to the Van der Waals attraction forces between nanoparticles (Phanthong et al. 2018).

The TEM image of NC-Cu^{2+}PANI morphology shows that more portions appear thick and dark cloudy region represents the amorphous nature as shown in Figure 9(g, h, i). The image shows thick dark region due to copper nano particles agglomerated in a PANI rod-like structure as shown in Figure 9(g, h and i), and the increased magnitude dispersion of NC-Cu^{2+} on the PANI matrix is as shown in figure. It is observed from Figure 9(g, h, and i) that rod-like NC-Cu^{2+}PANI are about 50–300 nm in length and about 4–15 nm in width. The thick dark region embedded on surface of white background which indicates there is a presence of a greater number of copper metal ions (Ashokkumar et al. 2020).

Fourier transform infrared spectroscopy (FT-IR)

The FT-IR spectra of the NCs, NC-Cu^{2+} and NC-Cu^{2+}PANI nanocomposites are shown in Figures 10–12 respectively.

For the determination of functional groups, FTIR spectra were shown in Figures 10–12. According to Figure 10, the synthesized NCs showed the bands at the peaks at 3317 cm^{-1}, 2891 cm^{-1}, and 1610 cm^{-1} that are attributed to the stretching vibrations of OH, C-H, and C-O, respectively. The IR spectra of NC-Cu^{2+} in Figure 11 shows the broad peak at 3336 cm^{-1} and weak peak at 1641 cm^{-1}. These are assigned to the stretching and bending vibrations of hydroxyl groups besides the metal oxide nanoparticles.

NC-Cu^{2+}PANI shows the characteristic absorption peak of OH at 3336 cm^{-1}, and the CH stretching vibration is observed at 2897 cm^{-1} as can see based on Figure 12. The absorption peaks at 1639 and 1539 cm^{-1} are assigned to the bending vibration of C-O and CH_2 stretching, respectively. The in-situ polymerization of NC-Cu^{2+} with PANI slightly affects the shift of the absorption peak. The composite shows new absorption peaks at 1321 cm^{-1}, and these bands are attributed to the presence of NC-Cu^{2+} in the PANI matrix. The shift in wave number of the composite is due to the interfacial interactions between the nanoparticles and the PANI matrix. Thus, we can conclude that monomer molecules are uniformly adsorbed on the surface of NC-Cu^{2+} nanoparticles.

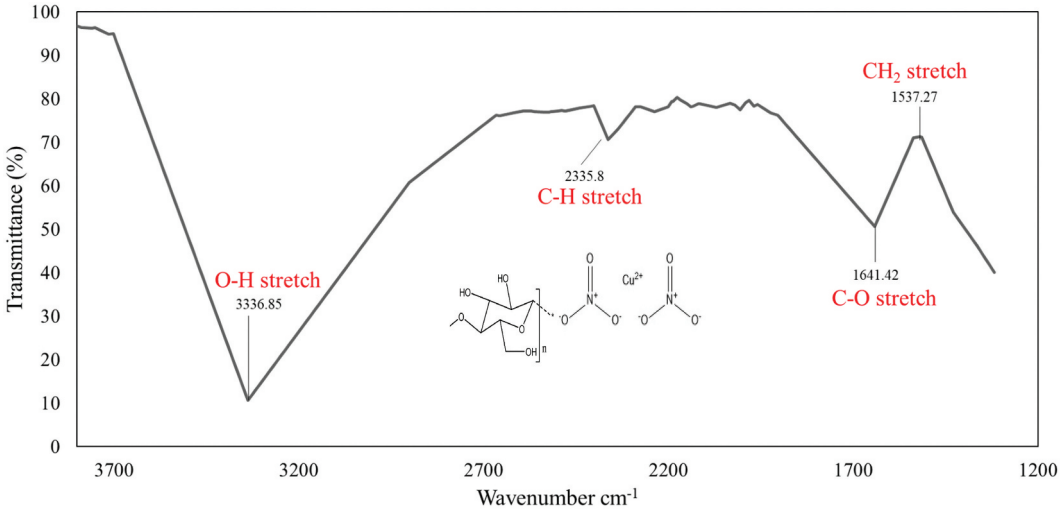

Figure 11. FT-IR of NC-Cu^{2+}.

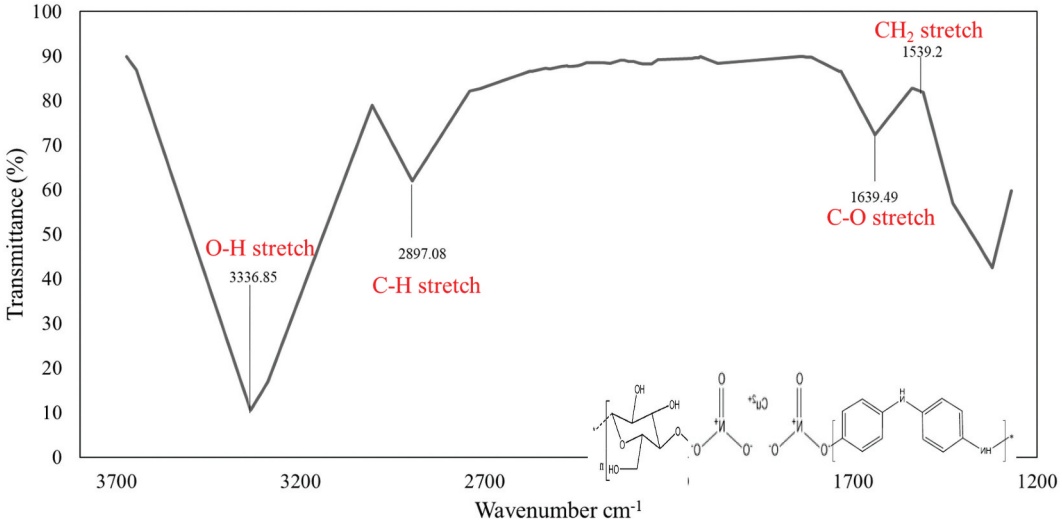

Figure 12. FT-IR of NC-Cu^{2+}PANI.

Thermogravimetric analysis (TGA)

The thermogravimetric curves of NCs, NC-Cu^{2+} and NC-Cu^{2+}PANI are illustrated in Figure 13.

Based on Figure 13, it shows that three consecutive steps of weight loss are obtained for NCs, NC-Cu^{2+} and NC-Cu^{2+}PANI. The first slight weight loss of all materials results from the water evaporation at around 100°C and is related to the loss of free, adsorbed and interlayer water. The middle weight loss between 200°C and 320°C is associated with the removal of unreacted monomers and oligomers. The final weight loss from 430°C is assigned to the decomposition of the polymer backbone. According to Figure 13, NCs, NC-Cu^{2+} and NC-Cu^{2+}PANI showed same weight loss when the temperature raised to 100°C due to the evaporation of water content. However, the NC-Cu^{2+}PANI nanocomposite showed significant weight loss of when the temperature raised to 200°C due to the evaporation of water residues. At 225°C, there was a sharp weight loss resulting from thermal decomposition of the pyrolysis of NC-Cu^{2+}PANI. When the temperature was raised to 350°C, NC-Cu^{2+}PANI showed a small weight loss due to the decomposition of organic matter of the nanocomposite (NC-Cu^{2+} and polyaniline). This indicates that the metal oxide nanoparticles impart better thermal resistance to PANI, and this is mainly attributed to the enhanced interfacial interaction between nanoparticles and the PANI. There is also a clear relation between the

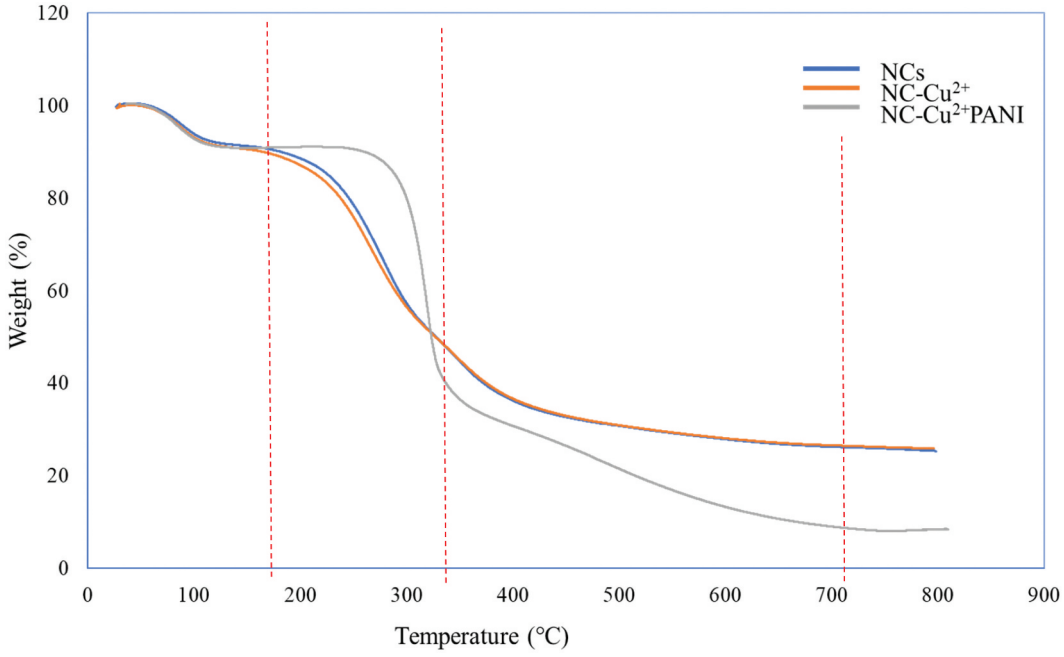

Figure 13. Thermogravimetric analysis (TGA) of NCs, NC-Cu^{2+} and NC-Cu^{2+}PANI.

morphologies and the thermal properties of composite. Subsequently, the decomposition of organic matter was started above 225°C and completed at 700°C. The TGA results indicated the high thermal stability of the synthesized NC-Cu^{2+}PANI nanocomposite. We can conclude that the combination between NCs and Cu^{2+} enhances the composite thermal stability.

Batch adsorption technique

Initial concentration

Figure 14 depicts the effect on concentration of Cu^{2+}. Keeping the amount of NCs (0.5 g) and constant rotation (70 rpm), the effect of changes in the initial concentration of metal ions on the amount of adsorbent was studied.

The adsorbed ions decreased with an increase in the concentration of the Cu^{2+} used. The adsorbent for the metal ions in solution is high at low ion concentrations, so metal ions interact with the adsorbent and were removed from the solution. The concentration gradient is stronger at high concentrations and the amount of equilibrium adsorption, q_e (*mg/l*), is low (Madivoli et al. 2016).

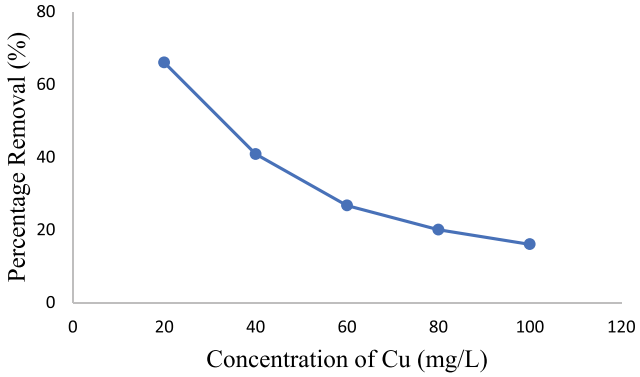

Figure 14. Effect on concentration of Cu^{2+}.

The effect of the initial concentration factor depends on the immediate relationship between the concentration and the available binding sites on the adsorbent surface. Generally, the percentage of removal decreases with an increase in the initial concentration, which may be due to saturation of adsorption sites on the adsorbent surface and increased adsorption capacity with an increase in the copper concentration (Banerjee et al. 2012). At low concentrations, active sites on the adsorbent surface will be unoccupied and when the initial concentration increases, the active sites required for molecular adsorption will not be available (Pathania, Sharma, and Singh 2017). In addition, the percentage of adsorption decreased with an increase in the initial concentration and increased as the contact time lasted. However, the increase in the initial concentration caused an increase in the loading capacity of the adsorbent and this may be due to the high driving force of the mass at a high initial concentration (BH B. Hameed, Krishni, and Sata 2009). In other words, higher in metal concentrations, the residual concentration of molecules will be higher. In the case of lower concentrations, the ratio of the initial number of molecules to the available adsorption sites is low and the fractional adsorption is subsequently independent of the initial concentration (Etim, Umoren, and Eduok 2016).

The percentage of removal is highly dependent on the initial concentration. The effect of the initial concentration factor depends on the immediate relationship between the concentration and the available binding sites on the adsorbent surface. Generally, the percentage of removal decreases with an increase in the initial concentration, which may be due to saturation of adsorption sites on the adsorbent surface and increased adsorption capacity with an increase in the initial copper concentration M. A. M. Salleh et al. (2011). At low concentrations, active sites on the adsorbent surface will be unoccupied and when the initial concentration increases, the active sites required for molecular adsorption will not be available (Pathania, Sharma, and Singh 2017). In addition, the percentage of adsorption decreased with an increase in the initial concentration and increased as the contact time lasted (Yu et al. 2000). However, the increase in the initial concentration caused an increase in the loading capacity of the adsorbent and this may be due to the high driving force of the mass at a high initial concentration (BH B. Hameed, Krishni, and Sata 2009). In other words, for higher initial metal concentrations, the residual concentration of molecules will be higher. In the case of lower concentrations, the ratio of the initial number of molecules to the available adsorption sites is low and the fractional adsorption is subsequently independent of the initial concentration (Etim, Umoren, and Eduok 2016).

Contact time

Figure 15 reveals the percentage removal of Cu^{2+} based on the contact time. The effect of contact time on Cu^{2+} adsorption was investigated at 0.5 g and 20 ppm for a fixed dose of NCs and initial concentration of Cu^{2+}, respectively. Figure 15 describes the percentage of Cu^{2+} removed over the course of 3 hours.

From Figure 15, the equilibrium is attained after approximately 120 min. From the figure also, the Cu^{2+} was rapidly adsorbed in the first 10 min for adsorbent with lower impregnation ratio and then the

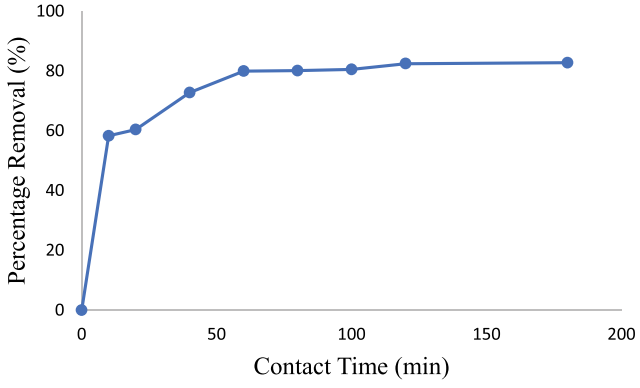

Figure 15. Effect of contact time.

adsorption rate increases gradually and reached equilibrium in after 110 min. At the beginning, the surface area of NCs has not yet occupied. The Cu^{2+} was adsorbed by the exterior surface of the NCs. At the beginning, the rate of adsorption was fast initially. Once the exterior surface occupied by the dye ions and saturated, the Cu^{2+}entered the pores of the adsorbent particles and was adsorbed by the interior surface of the particle. This phenomenon takes a relatively long contact time until the interior surface is also saturated and causes an equilibrium rate attained in the adsorption (Yashim and Marjohan 2006). Kadirvelu, Faur-Brasquet, and Cloirec (2000) suggested that by giving sufficient time of contact will allow color particles to penetrate the pores of carbon completely and fully saturates the active surfaces. This feature can be attributed to the high surface area of the sample and the large number of active functional groups for the complexation of metal ions, which are readily available to metal ions. As time passes, the adsorption centers gradually fill up and the intracellular ions penetrate through the adsorbed ions and become more difficult to bond to the vacancies (X. Chen et al. 2021).

pH

Figure 16 illustrates the percentage removal of Cu^{2+} on different pH value (2–10).

Since the ionization constants of the various hydroxyl groups are reported to be in the pH range 3–4, the biosorption of metal ions reversibly increases as the pH of the solution increases and the surface of the bio sorbent acquires a more negative charge due to the ionization of hydroxyl groups. Several researchers have also investigated the effect of pH on the biosorption of heavy metals using various bio sorbents (Abdi and Kazemi 2015). The biosorption of Cu^{2+} has been found to be in the range 6 in this research.

In acidic pH range (2–6), positively charged active surface on the activated carbon increases and thus attracts the negatively charged functional groups on the reactive Cu^{2+}, leading to maximum uptake within this range. As the pH of the solution increases, the number of negatively charged surfaces increases and competes with the positively charged surfaces sites.

Adsorbent dosage

The effect of the adsorbent dosage on adsorption of Cu^{2+} was tested at five different dosages: 0.5 g, 1 g, 2 g, 3 g and 4 g as described in Figure 17. Figure 17 represents the percentage of copper ions that were removed as the amount of adsorbent increased.

The amount of adsorbent is an important parameter that determines the adsorption capacity of the adsorbent for a given initial concentration. Increasing the amount of adsorbent due to the very high surface area of the sample increases the number of active sites for the complexation of metal ions and increases the adsorption process (Soliman and Moustafa 2020). Based on Figure 17, it can be said that the adsorption rate initially increases with increasing adsorbent dosage and then decreases. The increase in adsorption efficiency by increasing the amount of adsorbent can be attributed to the amine groups at the adsorbent surface which react with Cu^{2+} due to the complexation mechanism and play a very important role in their

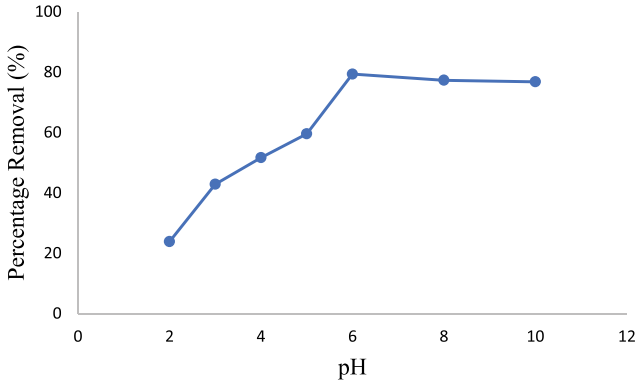

Figure 16. Effect on pH.

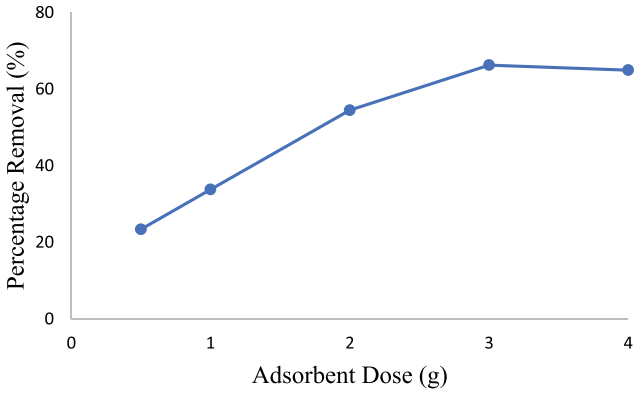

Figure 17. Effect of adsorbent dosage.

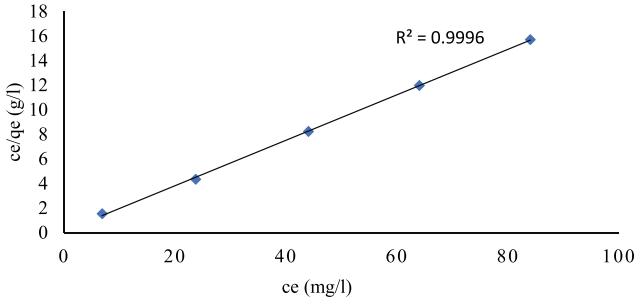

Figure 18. Langmuir Isotherm of adsorption of Cu^{2+} onto absorbent.

removal from aqueous solution (S. Chen et al. 2010). As the adsorbent increases further, the adsorption capacity decreases. The decrease in adsorption capacity of Cu^{2+} by increasing the amount of adsorbent is due to the increased interference between the bonding sites at higher amounts of adsorbent or the inability of metal ions in solution relative to the bonding sites (Alipour et al. 2020).

Adsorption isotherm

This section will discuss on the adsorption isotherm involved in the adsorption of Cu^{2+} on the NCs. Adsorption isotherms describe the existence of adsorbate between the liquid and solid phase. Position of equilibrium is determined by the distribution ratio of the solute between the liquid and the solid phase.

Langmuir isotherm

The interaction between the adsorbent surface and toxic particles can be well-interpreted by the study of the adsorption isotherms. The two isotherms' models Freundlich and Langmuir were used to study the experimental data of Cu^{2+} removal on the surface of NCs. It is well-known that Freundlich isotherm suggests the exponential distribution of the adsorption sites as well as the heterogeneous properties of the surface while the Langmuir isotherm suggests the presence of finite amount of identical adsorption sites on the surface of adsorbent as well as the formation of monolayer of adsorbates (Ituen, Akaranta, and James 2017). The fitting of experimental data of Langmuir and Freundlich isotherm models are shown in Figures 18 and 19 and their parameters were tabulated in Tables 4 and 5.

The linear plots of C_e/q_e vs. Ce showed that the adsorption obeys Langmuir isotherm. The values of K_L and R_L were determined for Cu^{2+} adsorption from intercept and slopes of the linear plots of Langmuir isotherm respectively.

Table 4 shows the good fit of the experimental data and the correlation coefficient (R^2) higher than 0.89 indicates the applicability of the Langmuir isotherm model (Tan, Ahmad, and Hameed 2008). R_L values for Cu^{2+} adsorption is shown in Table 4, and it was found that value of R_L is observed to be in the range 0–1,

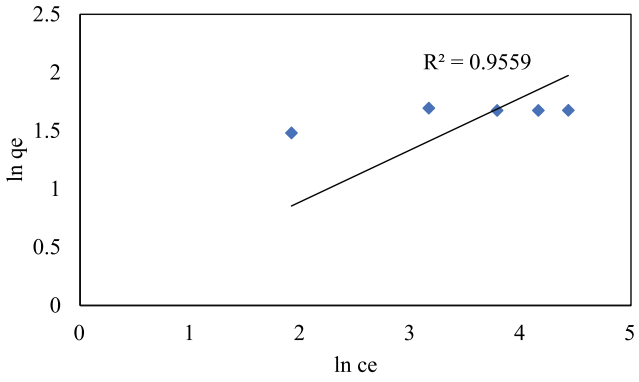

Figure 19. Freundlich Isotherm of adsorption of Cu^{2+} onto adsorbent.

Table 4. Langmuir isotherm adsorption constant for Cu^{2+}.

Langmuir isotherm			
qmax(mg/g)	K_L	R_L	R^2
79.491	0.0283	0.6384	0.9996

Table 5. Freundlich isotherm constant for Cu^{2+}.

Freundlich isotherm		
1/*n*	K_F	R^2
0.53009	3.3891	0.9559

indicating that the adsorption process is favorable using NCC. The R_L value of Cu^{+2} is 0.6384, accordingly, adsorption of Cu^{+2} is appropriately modeled with Langmuir isotherm.

Freundlich isotherm

Figure 19 shows a straight line with a slope of 1/*n* and intercept of ln (K_F) when *ln* (q_e) is plotted against *ln* (C_e).

Correlation coefficient (R^2) calculated from Freundlich isotherm for adsorbent is above 0.9559 (Table 5).

From the value of slope and intercept of the Freundlich isotherm, value of 1/n ranging between 0 and 1 indicates the surface heterogeneity (B. H. Hameed, Ahmad, and Latiff 2007). Decreasing impregnation ratio, the value of 1/n gets closer to zero which indicates that the surface becomes more heterogeneous with decreasing impregnation ratio (B. H. Hameed, Ahmad, and Latiff 2007). The correlation coefficients R (0.9996 and 0.9559 for Langmuir and Freundlich, respectively) revealed good agreement between experimental data and theoretical models. The Langmuir isotherm, however, fits better with the experimental data compared to Freundlich isotherm as the correlation coefficient (R) is much higher. All the constant for both isotherms correlated suggest that Cu^{2+} favorably adsorbed by NCs.

Adsorption kinetics

The plot for Pseudo-first order and Pseudo-second order were illustrated in Figures 20 and 21. The coefficient of correlation for the kinetics model for Pseudo-first order, Pseudo-second order and calculated value of second-order rate constant and correlation coefficient were tabulated in Table 6.

From Table 6, value for calculated equilibrium adsorption capacity (*qe* calc.) for the pseudo-second-order kinetic model is more consistent compared to first-order kinetic model.

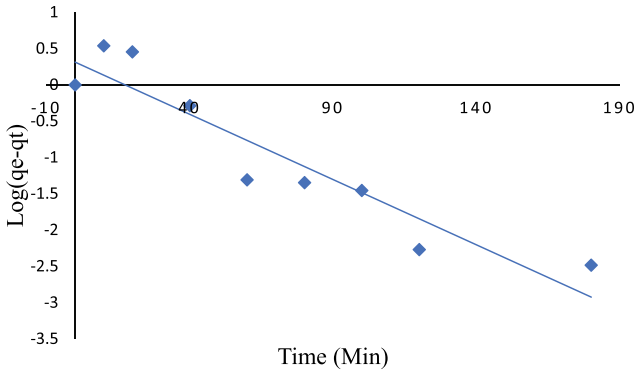

Figure 20. Pseudo-first-order kinetics for the adsorption of Cu^{2+} onto adsorbent.

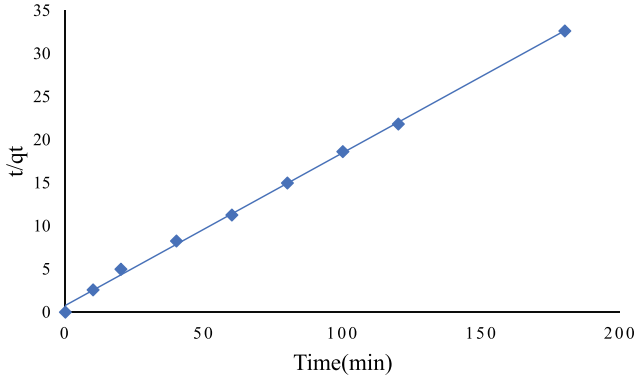

Figure 21. Pseudo-second-order kinetics for the adsorption of Cu^{2+} onto adsorbent.

Table 6. Comparison of the pseudo-first- and second-order adsorption rate constant and correlation coefficient.

Adsorbent	q_e (exp)	First -order kinetic model			Second- order kinetic model		
	(mg/g)	k_1	q_e (calc.)(mg/g)	R^2	k_2	q_e (calc.)(mg/g)	R^2
	4.4	-0.008	0.62	0.9092	0.32	23.6	0.9985

Table 7. Conductivity of the NC-Cu^{2+}PANI nanocomposites.

PANI/NCC-Cu ratio	Conductivity Values (S/cm^{-1})
Pure PANI	3.53
1:9	8.27
2:8	7.31
3:7	5.73

The correlation coefficient (R^2) for pseudo-second-order adsorption model has higher value compared to first-order adsorption model, suggesting that the pseudo-second-order adsorption mechanism is more dominant and overall rate of Cu^{2+} adsorption is controlled by chemisorption process (B. H. Hameed, Ahmad, and Latiff 2007).

Conducting polymer composites of NC-Cu^{2+}PANI

Table 7 shows the conductivity of the NC-Cu^{2+}PANI nanocomposites. The conductivity of the nanocomposite can be considered to arise from macroscopic and microscopic factors. The conductivity can be controlled by the composition and type of doping materials, processing conditions, conjugation length and chain length. The conductivity of the nanocomposites (NC-Cu^{2+}PANI) is higher than pure PANI and the

Table 8. A comparative data on electrical and mechanical properties of nanocomposites based on the PANI and cellulose/nanocellulose.

Sample Name/electrode type	Technique of Polymerization of PANI	Conductivity, S/cm^{-1}	Reference
CNCs/PANI composites	In- situ polymerization controlled by open circuit potential adjustment	8.9×10^{-1}	(Nepomuceno et al. 2021)
Cellulose/polyphenylacetylene/PANI triple-layered composite membrane	In -situ polymerization	6.5×10^{-4}	(Yatsu and Goto 2021)
Cellulose paper coated with CNC/PANI composites	Emulsion polymerization	5.64 S/m with 8 wt% coated paper	(Huang et al. 2021)
Cotton textiles/PANI nanocomposites	In-situ polymerization	–	(Tissera et al. 2018)
Paper coated with NFC/Ag/PANI nanocomposite	In -situ polymerization	Maximum of 0.0167 S/m, when amount of coating was 25.2 g/m^2	(K. Liu et al. 2018)
NCC/Cu^{2+}/PANI	In- situ polymerization	8.27×10^{-1}	Current research

conductivity goes on decreasing as increase in wt.% of NC-Cu^{2+} nanoparticles. As shown in Table 7, the conductivity of the NC-Cu^{2+}PANI nanocomposite is recorded in the range of 5.73–18.27 × 10 S/cm^{-1}, which is significantly higher than that of the pure PANI (3.53 ×10 S/cm^{-1}) and the conductivity decreased with increase of the NC-Cu^{2+} -to-PANI ratio.

The decrease in conductivity is due to macroscopic contribution, which affects the density of the nanocomposite. This is reflected as NC-Cu^{2+} nanoparticles embedded in the PANI matrix act as particles blockage of conducting path in the PANI-Chain. Hence, decrease in conductivity is observed as increase in content of NC-Cu^{2+} nanoparticles in PANI matrix. The in-situ polymerization of the aniline monomer on the surface of metal oxide nanoparticles leads to the uniform distribution of nanoparticles in the PANI matrix.

As shown in Table 7, the maximum conductivity is obtained for 1:9 ratio. The percolation threshold, i.e., the critical filler loading at this concentration of nanoparticle, is due to the strong interfacial interaction between the PANI and the nanoparticles. The interfacial interactions would increase the orientation of nanoparticles within the PANI and thereby improve the quality of the electrical network formation. It is known that the electrical conductivity of a polymer composite depends on the interfacial polarization between the nanoparticles, the polymer chain, and the uniform dispersion of nanoparticles (Ramesan et al. 2018). Table 8 shows a comparative data on electrical and mechanical properties of nanocomposites based on the PANI and cellulose/nanocellulose.

Conclusion

This study demonstrates a green and straightforward route to synthesize a nanocellulose/Cu^{2+} (NCs/Cu^{2+}) – polyaniline nanocomposite. Cellulose was first hydrolyzed with sulfuric acid to obtain nanocellulose, which was subsequently functionalized with polyaniline via in-situ polymerization. Structural and physicochemical characterization confirmed successful nanocomposite formation: XRD patterns indicated increased structural ordering in the presence of NC – Cu^{2+}; TEM images revealed rod-like NC – Cu^{2+} –PANI structures with copper ions distributed on the surface; FTIR spectra showed slight peak shifts associated with interaction between NC – Cu^{2+} and PANI; and TGA confirmed high thermal stability. Batch adsorption studies showed excellent agreement between experimental data and isotherm models, with correlation coefficients of 0.9996 (Langmuir) and 0.9559 (Freundlich), and a better fit to the Langmuir model. The adsorption kinetics followed a pseudo-second-order model, indicating chemisorption as the dominant mechanism. The NC – Cu^{2+} –PANI nanocomposite exhibited significantly higher conductivity (5.73–18.27 × 10 S cm^{-1}) than pure PANI (3.53 × 10 S cm^{-1}), with conductivity decreasing as the NC – Cu^{2+} :PANI ratio increased. Under optimal conditions (pH 6.0, contact time ≈120 min, initial Cu^{2+} concentration 20 mg L^{-1}), the nanocomposite achieved substantial removal of Cu^{2+} ions. Overall, the developed adsorbent shows strong potential for wastewater treatment applications and provides a versatile platform for further optimization and extension to other heavy metal pollutants.

Acknowledgments

The authors would like to express gratitude for the financial support received from the Geran Putra-Inisiatif Putra Muda (GP-IPM) (GP-IPM/2023/9773300).

Author contributions

Conceptualization, writing-original draft preparation, review and editing: Nur Athirah Abdullah, Mohd Saiful Asmal Rani, Masita Mohammad; Conceptualization: Muhamad Fadhli Ramlee, Rushdan Ahmad Ilyas. All authors have accepted responsibility for the entire content of this manuscript and approved its submission.

Disclosure statement

No potential conflict of interest was reported by the author(s).

Funding

Geran Putra-Inisiatif Putra Muda (GP-IPM) [GP-IPM/2023/9773300].

References

Aasli, B., N. El Messaoudi, A. El Mouden, M. El-Habacha, G. Mahmoudy, Y. Miyah, A. Lacherai, S. Knani, and A. Lacherai. 2025. "Synthesis of Urea-Formaldehyde Resin@ Chitosan Composite for the Removal of Congo Red from an Aqueous Solution via Adsorption: Box-Behnken Design Optimization." *International Journal of Biological Macromolecules* 315:144648. https://doi.org/10.1016/j.ijbiomac.2025.144648.

Abdi, O., and M. Kazemi. 2015. "A Review Study of Biosorption of Heavy Metals and Comparison Between Different Biosorbents." *Journal of Materials and Environmental Science* 6 (5): 1386–1399.

Abouzeid, R. E., R. Khiari, N. El-Wakil, and A. Dufresne. 2018. "Current State and New Trends in the Use of Cellulose Nanomaterials for Wastewater Treatment." *Biomacromolecules* 20 (2): 573–597. https://doi.org/10.1021/acs.biomac.8b00839.

Afroze, S., and T. K. Sen. 2018. "A Review on Heavy Metal Ions and Dye Adsorption from Water by Agricultural Solid Waste Adsorbents." *Water, Air, & Soil Pollution* 229 (7): 1–50. https://doi.org/10.1007/s11270-018-3869-z.

Ahamad, Z., and A. Nasar. 2025. "Conjugated Polymers Decorated Lignocellulosicnanocomposites for Malachite Green Contaminated Water Remediation." *Separation andPurification Technology* 354:128688. https://doi.org/10.1016/j.seppur.2024.128688.

Alipour, A., S. Zarinabadi, A. Azimi, and M. Mirzaei. 2020. "Adsorptive Removal of Pb (II) Ions from Aqueous Solutions by Thiourea-Functionalized Magnetic ZnO/Nanocellulose Composite: Optimization by Response Surface Methodology (RSM)." *International Journal of Biological Macromolecules* 151:124–135. https://doi.org/10.1016/j.ijbiomac.2020.02.109.

Ashokkumar, S. P., H. Vijeth, L. Yesappa, M. Niranjana, M. Vandana, and H. Devendrappa. 2020. "Electrochemically Synthesized Polyaniline/Copper Oxide Nano Composites: To Study Optical Band Gap and Electrochemical Performance for Energy Storage Devices." *Inorganic Chemistry Communications* 115:107865. https://doi.org/10.1016/j.inoche.2020.107865.

Banerjee, K., S. T. Ramesh, R. Gandhimathi, P. V. Nidheesh, and K. S. Bharathi. 2012. "A Novel Agricultural Waste Adsorbent, Watermelon Shell for the Removal of Copper from Aqueous Solutions." *Iranica Journal of Energy & Environment* 3 (2): 143–156.

Barbosa, V., Jr, E. C. Ramires, I. A. T. Razera, and E. Frollini. 2010. "Biobased Composites from Tannin–Phenolic Polymers Reinforced with Coir Fibers." *Industrial Crops and Products* 32 (3): 305–312. https://doi.org/10.1016/j.indcrop.2010.05.007.

Chen, S., W. Shen, F. Yu, W. Hu, and H. Wang. 2010. "Preparation of Amidoximated Bacterial Cellulose and Its Adsorption Mechanism for Cu2+ and Pb2+." *Journal of Applied Polymer Science* 117 (1): 8–15. https://doi.org/10.1002/app.31477.

Chen, X., Z. Tian, H. Cheng, G. Xu, and H. Zhou. 2021. "Adsorption Process and Mechanism of Heavy Metal Ions by Different Components of Cells, Using Yeast (Pichia pastoris) and Cu 2+ as Biosorption Models." *RSC Advances* 11 (28): 17080–17091. https://doi.org/10.1039/D0RA09744F.

Chieng, B. W., S. H. Lee, N. A. Ibrahim, Y. Y. Then, and Y. Y. Loo. 2017. "Isolation and Characterization of Cellulose Nanocrystals from Oil Palm Mesocarp Fiber." *Polymers* 9 (8): 355. https://doi.org/10.3390/polym9080355.

Clauser, N. M., G. González, C. M. Mendieta, J. Kruyeniski, M. C. Area, and M. E. Vallejos. 2021. "Biomass Waste as Sustainable Raw Material for Energy and Fuels." *Sustainability* 13 (2): 794. https://doi.org/10.3390/su13020794.

Collazo-Bigliardi, S., R. Ortega-Toro, and A. C. Boix. 2018. "Isolation and Characterisation of Microcrystalline Cellulose and Cellulose Nanocrystals from Coffee Husk and Comparative Study with Rice Husk." *Carbohydrate Polymers* 191:205–215. https://doi.org/10.1016/j.carbpol.2018.03.022.

Dutta, S., J. Kim, Y. Ide, J. H. Kim, M. S. A. Hossain, Y. Bando, Y. Yamauchi, and K. C.-W. Wu. 2017. "3D Network of Cellulose-Based Energy Storage Devices and Related Emerging Applications." *Materials Horizons* 4 (4): 522–545.

El Messaoudi, N., Y. Miyah, N. Singh, S. Gubernat, R. Fatima, J. Georgin, A. El Mouden, S. Saghir, S. Knani, and Y. Hwang. 2024. "A Critical Review of Allura Red Removal from Water: Advancements in Adsorption and Photocatalytic Degradation Technologies, and Future Perspectives." *Journal of Environmental Chemical Engineering* 12 (6): 114843. https://doi.org/10.1016/j.jece.2024.114843.

El Messaoudi, N., Y. Miyah, W. A. A. Q. I. Wan, Z. M. Hanafiah, J. O. Ighalo, E. C. Emenike, J. Georgin, et al. 2024. "Advancements in Adsorption and Photocatalytic Degradation Technologies of Brilliant Green from Water: Current Status, Challenges, and Future Prospects." *Materials Today Chemistry* 42:102399. https://doi.org/10.1016/j.mtchem.2024.102399.

Etim, U. J., S. A. Umoren, and U. M. Eduok. 2016. "Coconut Coir Dust as a Low Cost Adsorbent for the Removal of Cationic Dye from Aqueous Solution." *Journal of Saudi Chemical Society* 20:S67–S76. https://doi.org/10.1016/j.jscs.2012.09.014.

Fan, X.-M., H.-Y. Yu, D.-C. Wang, Z.-H. Mao, J. Yao, and K. C. Tam. 2019. "Facile and Green Synthesis of Carboxylated Cellulose Nanocrystals as Efficient Adsorbents in Wastewater Treatments." *ACS Sustainable Chemistry & Engineering* 7 (21): 18067–18075. https://doi.org/10.1021/acssuschemeng.9b05081.

Fei, G., Y. Wang, H. Wang, Y. Ma, Q. Guo, W. Huang, D. Yang, Y. Shao, and Y. Ni. 2019. "Fabrication of Bacterial Cellulose/Polyaniline Nanocomposite Paper with Excellent Conductivity, Strength, and Flexibility." *ACS Sustainable Chemistry & Engineering* 7 (9): 8215–8225. https://doi.org/10.1021/acssuschemeng.8b06306.

Gupta, G., M. Baranwal, S. Saxena, and M. S. Reddy. 2022. "Utilization of Banana Waste as a Resource Material for Biofuels and Other Value-Added Products." *Biomass Conversion and Biorefinery* 13 (14): 1–20. https://doi.org/10.1007/s13399-022-02306-6.

Hameed, B. H., A. L. Ahmad, and K. N. A. Latiff. 2007. "Adsorption of Basic Dye (Methylene Blue) Onto Activated Carbon Prepared from Rattan Sawdust." *Dyes and Pigments* 75 (1): 143–149. https://doi.org/10.1016/j.dyepig.2006.05.039.

Hameed, B., R. R. Krishni, and S. A. Sata. 2009. "A Novel Agricultural Waste Adsorbent for the Removal of Cationic Dye from Aqueous Solutions." *Journal of Hazardous Materials* 162 (1): 305–311. https://doi.org/10.1016/j.jhazmat.2008.05.036.

Haque, S., D. Akbar, and S. Kinnear. 2020. "The Variable Impacts of Extreme Weather Events on Fruit Production in Subtropical Australia." *Scientia Horticulturae* 262:109050. https://doi.org/10.1016/j.scienta.2019.109050.

Höfer, R. 2015. "Sugar-and Starch-based Biorefineries." *Industrial Biorefineries and White Biotechnology*: 157–235. https://books.google.com.my/books?hl=en&lr=&id=dxKdBAAAQBAJ&oi=fnd&pg=PA157&dq=Sugar-and+Starch-based+Biorefineries.%E2%80%9D+Industrial+Biorefineries+and+White+Biotechnology:+157%E2%80%93235.&ots=d_7oJmLKbm&sig=ope_mFnsbvS5IdeeYh72gq-UiKw&redir_esc=y#v=onepage&q&f=false.

Hu, L., H. Du, C. Liu, Y. Zhang, G. Yu, X. Zhang, C. Si, B. Li, and H. Peng. 2018. "Comparative Evaluation of the Efficient Conversion of Corn Husk Filament and Corn Husk Powder to Valuable Materials via a Sustainable and Clean Biorefinery Process." *ACS Sustainable Chemistry & Engineering* 7 (1): 1327–1336. https://doi.org/10.1021/acssuschemeng.8b05017.

Huang, M., Y. Tang, X. Wang, P. Zhu, T. Chen, and Y. Zhou. 2021. "Preparation of Polyaniline/Cellulose Nanocrystal Composite and Its Application in Surface Coating of Cellulosic Paper." *Progress in Organic Coatings* 159:106452. https://doi.org/10.1016/j.porgcoat.2021.106452.

Ituen, E., O. Akaranta, and A. James. 2017. "Evaluation of Performance of Corrosion Inhibitors Using Adsorption Isotherm Models: An Overview." *Chemical Science International Journal* 18 (1): 1–34. https://doi.org/10.9734/CSJI/2017/28976.

Jain, A., D. Rastogi, and B. Chanana. 2022. "Product Development Using Cornhusk Fibres—A Sustainable Initiative." In *Sustainable Approaches in Textiles and Fashion*, 251–274. Springer.

Kaboorani, A., and B. Riedl. 2015. "Surface Modification of Cellulose Nanocrystals (CNC) by a Cationic Surfactant." *Industrial Crops and Products* 65:45–55. https://doi.org/10.1016/j.indcrop.2014.11.027.

Kadirvelu, K., C. Faur-Brasquet, and P. L. Cloirec. 2000. "Removal of Cu (II), Pb (II), and Ni (II) by Adsorption onto Activated Carbon Cloths." *Langmuir* 16 (22): 8404–8409. https://doi.org/10.1021/la0004810.

Khan, S., Z. Ahamad, and A. Nasar. 2025. "Lignocellulosic Juglans Regia Waste-Derived Magnetically Separable Nanocomposite for Enhanced Malachite Green Dye Removal." *International Journal of Biological Macromolecules* 318:144989. https://doi.org/10.1016/j.ijbiomac.2025.144989.

Khoo, R. Z., H. Ismail, and W. S. Chow. 2016. "Thermal and Morphological Properties of Poly (Lactic Acid)/Nanocellulose Nanocomposites." *Procedia Chemistry* 19:788–794. https://doi.org/10.1016/j.proche.2016.03.086.

Köse, K., M. Mavlan, and J. P. Youngblood. 2020. "Applications and Impact of Nanocellulose Based Adsorbents." *Cellulose* 27 (6): 2967–2990. https://doi.org/10.1007/s10570-020-03011-1.

Lani, N. S., N. Ngadi, A. Johari, and M. Jusoh. 2014. "Isolation, Characterization, and Application of Nanocellulose from Oil Palm Empty Fruit Bunch Fiber as Nanocomposites." *Journal of Nanomaterials* 2014 (1). https://doi.org/10.1155/2014/702538.

Liu, C., B. Li, H. Du, D. Lv, Y. Zhang, G. Yu, X. Mu, and H. Peng. 2016. "Properties of Nanocellulose Isolated from Corncob Residue Using Sulfuric Acid, Formic Acid, Oxidative and Mechanical Methods." *Carbohydrate Polymers* 151:716–724. https://doi.org/10.1016/j.carbpol.2016.06.025.

Liu, D. Y., G. X. Sui, and D. Bhattacharyya. 2015. "Properties and Characterization of Electrically Conductive Nanocellulose-Based Composite Films." In *Fillers and Reinforcements for Advanced Nanocomposites*, edited by Y. Dong, R. Umer and A. K.-T. Lau, 3–25. Elsevier.

Liu, K., J. Nasrallah, L. Chen, L. Huang, Y. Ni, S. Lin, and H. Wang. 2018. "A Facile Template Approach to Preparing Stable NFC/Ag/Polyaniline Nanocomposites for Imparting Multifunctionality to Paper." *Carbohydrate Polymers* 194:97–102. https://doi.org/10.1016/j.carbpol.2018.04.015.

Madivoli, E., P. Kareru, A. Gachanja, S. Mugo, M. Murigi, P. K. Kairigo, C. Kipyegon, J. Mutembei, and F. Njonge. 2016. "Adsorption of Selected Heavy Metals on Modified Nano Cellulose." *International Research Journal of Pure and Applied Chemistry* 12 (3): 1–9. https://doi.org/10.9734/IRJPAC/2016/28548.

Mahfoudhi, N., and S. Boufi. 2017. "Nanocellulose as a Novel Nanostructured Adsorbent for Environmental Remediation: A Review." *Cellulose* 24 (3): 1171–1197. https://doi.org/10.1007/s10570-017-1194-0.

Malkapuram, R., V. Kumar, and Y. S. Negi. 2009. "Recent Development in Natural Fiber Reinforced Polypropylene Composites." *Journal of Reinforced Plastics and Composites* 28 (10): 1169–1189. https://doi.org/10.1177/0731684407087759.

Moberg, T., K. Sahlin, K. Yao, S. Geng, G. Westman, Q. Zhou, K. Oksman, and M. Rigdahl. 2017. "Rheological Properties of Nanocellulose Suspensions: Effects of Fibril/Particle Dimensions and Surface Characteristics." *Cellulose* 24 (6): 2499–2510. https://doi.org/10.1007/s10570-017-1283-0.

Mondal, S. 2018. "Review on Nanocellulose Polymer Nanocomposites." *Polymer-Plastics Technology and Engineering* 57 (13): 1377–1391. https://doi.org/10.1080/03602559.2017.1381253.

Monte, L. S., V. A. Escócio, A. M. F. de Sousa, C. R. G. Furtado, M. C. A. M. Leite, L. L. Y. Visconte, and E. B. A. V. Pacheco. 2018. "Study of Time Reaction on Alkaline Pretreatment Applied to Rice Husk on Biomass Component Extraction." *Biomass Conversion and Biorefinery* 8 (1): 189–197.

Morán, J. I., V. A. Alvarez, V. P. Cyras, and A. Vázquez. 2008. "Extraction of Cellulose and Preparation of Nanocellulose from Sisal Fibers." *Cellulose* 15 (1): 149–159. https://doi.org/10.1007/s10570-007-9145-9.

Narendar, R., and K. P. Dasan. 2014. "Chemical Treatments of Coir Pith: Morphology, Chemical Composition, Thermal and Water Retention Behavior." *Composites Part B: Engineering* 56:770–779. https://doi.org/10.1016/j.compositesb.2013.09.028.

Naz, S., J. S. Ali, and M. Zia. 2019. "Nanocellulose Isolation Characterization and Applications: A Journey from Non-remedial to Biomedical Claims." *Bio-Design and Manufacturing* 2 (3): 187–212. https://doi.org/10.1007/s42242-019-00049-4.

Nepomuceno, N. C., A. A. A. Seixas, E. S. Medeiros, and T. J. A. Mélo. 2021. "Evaluation of Conductivity of Nanostructured Polyaniline/Cellulose Nanocrystals (PANI/CNC) Obtained via in Situ Polymerization." *Journal of Solid State Chemistry* 302:122372. https://doi.org/10.1016/j.jssc.2021.122372.

Oyewo, O. A., B. Mutesse, T. Y. Leswifi, and M. S. Onyango. 2019. "Highly Efficient Removal of Nickel and Cadmium from Water Using Sawdust-Derived Cellulose Nanocrystals." *Journal of Environmental Chemical Engineering* 7 (4): 103251. https://doi.org/10.1016/j.jece.2019.103251.

Pathania, D., S. Sharma, and P. Singh. 2017. "Removal of Methylene Blue by Adsorption Onto Activated Carbon Developed from Ficus Carica Bast." *Arabian Journal of Chemistry* 10:S1445–S1451. https://doi.org/10.1016/j.arabjc.2013.04.021.

Phanthong, P., P. Reubroycharoen, X. Hao, G. Xu, A. Abudula, and G. Guan. 2018. "Nanocellulose: Extraction and Application." *Carbon Resources Conversion* 1 (1): 32–43. https://doi.org/10.1016/j.crcon.2018.05.004.

Pires, J. R., V. G. Souza, and A. L. Fernando. 2019. "Valorization of Energy Crops as a Source for Nanocellulose Production–Current Knowledge and Future Prospects." *Industrial Crops and Products* 140:111642. https://doi.org/10.1016/j.indcrop.2019.111642.

Ramesan, M. T. 2014. "Synthesis, Characterization, and Properties of New Conducting Polyaniline/Copper Sulfide Nanocomposites." *Polymer Engineering & Science* 54 (2): 438–445. https://doi.org/10.1002/pen.23572.

Ramesan, M. T., P. Jayakrishnan, T. Anilkumar, and G. Mathew. 2018. "Influence of Copper Sulphide Nanoparticles on the Structural, Mechanical and Dielectric Properties of Poly (Vinyl Alcohol)/Poly (Vinyl Pyrrolidone) Blend Nanocomposites." *Journal of Materials Science: Materials in Electronics* 29 (3): 1992–2000. https://doi.org/10.1007/s10854-017-8110-0.

Rashid, S., and H. Dutta. 2020. "Characterization of Nanocellulose Extracted from Short, Medium and Long Grain Rice Husks." *Industrial Crops and Products* 154:112627. https://doi.org/10.1016/j.indcrop.2020.112627.

Salado, M., S. Lanceros-Mendez, and E. Lizundia. 2021. "Free-Standing Intrinsically Conducting Polymer Membranes Based on Cellulose and Poly (Vinylidene Fluoride) for Energy Storage Applications." *European Polymer Journal* 144:110240. https://doi.org/10.1016/j.eurpolymj.2020.110240.

Salleh, M. A. M., D. K. Mahmoud, W. A. W. A. Karim, and A. Idris. 2011. "Cationic and Anionic Dye Adsorption by Agricultural Solid Wastes: A Comprehensive Review." *Desalination* 280 (1–3): 1–13.

Sangamesha, M. A., K. Pushpalatha, and G. L. Shekar. 2014. "Structural and Optical Studies of Conducting PANI/CuS Nanocomposites on Nanocrystalline Zinc-Oxide Thin Film." *American Journal of Nanotechnology* 5 (1): 3. https://doi.org/10.3844/ajnsp.2014.3.11.

Septevani, A. A., A. Rifathin, A. A. Sari, Y. Sampora, G. N. Ariani, S. Sondari, and D. Sondari. 2020. "Oil Palm Empty Fruit Bunch-Based Nanocellulose as a Super-Adsorbent for Water Remediation." *Carbohydrate Polymers* 229:115433. https://doi.org/10.1016/j.carbpol.2019.115433.

Shi, Y., L. Peng, Y. Ding, Y. Zhao, and G. Yu. 2015. "Nanostructured Conductive Polymers for Advanced Energy Storage." *Chemical Society Reviews* 44 (19): 6684–6696. https://doi.org/10.1039/C5CS00362H.

Siakeng, R., M. Jawaid, H. Ariffin, S. M. Sapuan, M. Asim, and N. Saba. 2019. "Natural Fiber Reinforced Polylactic Acid Composites: A Review." *Polymer Composites* 40 (2): 446–463. https://doi.org/10.1002/pc.24747.

Soliman, N. K., and A. F. Moustafa. 2020. "Industrial Solid Waste for Heavy Metals Adsorption Features and Challenges; a Review." *Journal of Materials Research and Technology* 9 (5): 10235–10253. https://doi.org/10.1016/j.jmrt.2020.07.045.

Song, Y., W. Jiang, Y. Zhang, H. Wang, F. Zou, K. Yu, and G. Han. 2018. "A Novel Process of Nanocellulose Extraction from Kenaf Bast." *Materials Research Express* 5 (8): 085032. https://doi.org/10.1088/2053-1591/aac80d.

Sun, J. X., X. F. Sun, H. Zhao, and R. C. Sun. 2004. "Isolation and Characterization of Cellulose from Sugarcane Bagasse." *Polymer Degradation and Stability* 84 (2): 331–339. https://doi.org/10.1016/j.polymdegradstab.2004.02.008.

Tan, I. A. W., A. L. Ahmad, and B. H. Hameed. 2008. "Adsorption of Basic Dye on High-Surface-Area Activated Carbon Prepared from Coconut Husk: Equilibrium, Kinetic and Thermodynamic Studies." *Journal of Hazardous Materials* 154 (1–3): 337–346. https://doi.org/10.1016/j.jhazmat.2007.10.031.

Tissera, N. D., R. N. Wijesena, S. Rathnayake, R. M. de Silva, and K. N. de Silva. 2018. "Heterogeneous in Situ Polymerization of Polyaniline (PANI) Nanofibers on Cotton Textiles: Improved Electrical Conductivity, Electrical Switching, and Tuning Properties." *Carbohydrate Polymers* 186:35–44. https://doi.org/10.1016/j.carbpol.2018.01.027.

Trache, D., M. H. Hussin, M. M. Haafiz, and V. K. Thakur. 2017. "Recent Progress in Cellulose Nanocrystals: Sources and Production." *Nanoscale* 9 (5): 1763–1786. https://doi.org/10.1039/C6NR09494E.

Trache, D., A. F. Tarchoun, M. Derradji, T. S. Hamidon, N. Masruchin, N. Brosse, and M. H. Hussin. 2020. "Nanocellulose: From Fundamentals to Advanced Applications." *Frontiers in Chemistry* 8:392. https://doi.org/10.3389/fchem.2020.00392.

Vakili, M., M. Rafatullah, M. H. Ibrahim, A. Z. Abdullah, B. Salamatinia, and Z. Gholami. 2014. "Oil Palm Biomass as an Adsorbent for Heavy Metals." *Reviews of Environmental Contamination and Toxicology* 232:61–88. https://doi.org/10.1007/978-3-319-06746-9.

Vardhan, K. H., P. S. Kumar, and R. C. Panda. 2019. "A Review on Heavy Metal Pollution, Toxicity and Remedial Measures: Current Trends and Future Perspectives." *Journal of Molecular Liquids* 290:111197. https://doi.org/10.1016/j.molliq.2019.111197.

Verma, D., P. C. Gope, A. Shandilya, A. Gupta, and M. K. Maheshwari. 2013. "Coir Fibre Reinforcement and Application in Polymer Composites." *Journal of Materials and Environmental Science* 4 (2): 263–276.

Vilarinho, F., A. Sanches-Silva, M. F. Vaz, and J. P. Farinha. 2017. "Nanocellulose: A Benefit for Green Food Packaging." *Critical Reviews in Food Science and Nutrition* 58 (9): 8398. https://doi.org/10.1080/10408398.2016.1270254.

Wang, R., S. Guan, A. Sato, X. Wang, Z. Wang, R. Yang, B. S. Hsiao, and B. Chu. 2013. "Nanofibrous Microfiltration Membranes Capable of Removing Bacteria, Viruses and Heavy Metal Ions." *Journal of Membrane Science* 446:376–382. https://doi.org/10.1016/j.memsci.2013.06.020.

Yang, X., F. Han, C. Xu, S. Jiang, L. Huang, L. Liu, and Z. Xia. 2017. "Effects of Preparation Methods on the Morphology and Properties of Nanocellulose (NC) Extracted from Corn Husk." *Industrial Crops and Products* 109:241–247. https://doi.org/10.1016/j.indcrop.2017.08.032.

Yashim, M. M., and E. L. Marjohan. 2006. "Adsorption Isotherm Study of Adsorption Methylene Blue Onto Oil Palm Kernel Shell Activated Carbon." *ARPN Journal of Engineering & Applied Sciences* 11 (20): 11907–11910.

Yatsu, A., and H. Goto. 2021. "Preparation of a Cellulose-Polyphenylacetylene-Polyaniline Composite." *The Journal of the Textile Institute* 112 (12): 1883–1889. https://doi.org/10.1080/00405000.2020.1867414.

Yu, B., Y. Zhang, A. Shukla, S. S. Shukla, and K. L. Dorris. 2000. "The Removal of Heavy Metal from Aqueous Solutions by Sawdust Adsorption—Removal of Copper." *Journal of Hazardous Materials* 80 (1–3): 33–42. https://doi.org/10.1016/S0304-3894(00)00278-8.

Zainudin, E. S., L. H. Yan, W. H. Haniffah, M. Jawaid, and O. Y. Alothman. 2014. "Effect of Coir Fiber Loading on Mechanical and Morphological Properties of Oil Palm Fibers Reinforced Polypropylene Composites." *Polymer Composites* 35 (7): 1418–1425. https://doi.org/10.1002/pc.22794.

Zhang, H., C. Dou, L. Pal, and M. A. Hubbe. 2019. "Review of Electrically Conductive Composites and Films Containing Cellulosic Fibers or Nanocellulose." *BioResources* 14 (3): 7494–7542. https://doi.org/10.15376/biores.14.3.7494-7542.